united nations
educational, scientific
and cultural
organization

international atomic
energy agency

the
abdus salam
international centre for theoretical physics

SMR 1161/9

AUTUMN COLLEGE ON PLASMA PHYSICS

25 October - 19 November 1999

Solar and Heliospheric Plasma Physics: Yesterday and Tomorrow Problems

Igor Veselovsky

Institute of Nuclear Physics
Moscow State University
Russia

These are preliminary lecture notes, intended only for distribution to participants.

Contents

" The restless Sun "

K.O. Kiepenheuer . 1957

The purpose of this lecture is to present an Introduction to the old ideas and possible future developments of the solar and heliospheric plasma physics. (See also lectures by E.Smith, V. Nakariakov, S. Poedts, B. Buti, M. Velli, A. Rogava).

The illustrative and descriptive style is preferred to avoid the author's bias when focusing on the observational facts and theoretical ideas.

To begin with, let us indicate several arbitrary sorted points of growth in the knowledge and understandi of solar and heliospheric phenomena.

Some problems

- Solar neutrino problem: astrophysical (standard model) and particle aspects
- solar radius and shape variations
- "solar constant" is not a constant. Why?
- solar cycle is not a just "toroidal - poloidal" magnetic field interplay, but what is it?
- solar interior rotation is revised and still under revision. Differential rotation.
- helioseismology is in rapid progress both observationally and theoretically
- why the "standard model" looks so accurate? mixing length, composition, opacity, outer boundary conditions, magnetic fields, oversimplified? steady-state?
- solar flares - essentially kinetic (non-MHD) phenomenon - very effective particle acceleration in small space-time scales.
- the same with the solar wind? coronal heating and solar wind acceleration
- regular and irregular (chaotic) components in the solar activity: from milliseconds, minutes, up to many years.

- Heliospheric (not solar!) origins of the interplanetary magnetic fields. The role of the heliospheric currents was underestimated and still not appreciated by many researchers. Heliospheric current sheets are main contributors to the field.
- The solar atmosphere is highly structured and dynamical. Processes in the chromosphere? in the transition region and the corona?
- Outer heliosphere structure? Termination shock: where? when? structure? Heliopause structure? Outer bow shock? Does it exist?
- Consequences of the low-degree ionisation in the outer heliosphere are not completly understood (interstellar gas)
- coronal mass ejections. Initiation and dynamics are under investigation

The energy, momentum and mass losses of the Sun are dominated by the light emission (and ν).
The solar wind part in these losses is small.
The comparison Light $\leftrightarrow$ Wind is presented in the Table

	Solar light	Solar Wind	Ratio
Energy flux density $\frac{\rho v^3}{2}$ erg/cm^{-2}s^{-1}	$1{,}4 \cdot 10^{6}$	0,4	$4 \cdot 10^{7}$
Momentum flux density ρv^2 (pressure) erg/cm^3	$5 \cdot 10^{-5}$	10^{-8}	$5 \cdot 10^{3}$
Momentum density ρv g(cm^{-2}s^{-1})	$1{,}7 \cdot 10^{-15}$	$2 \cdot 10^{-16}$	8

All quantities in the Table are referred to the distance 1 AU from the Sun (the Earth's orbit) and should be a factor $\times 4 \cdot 10^4$ greater at the Sun (distance 1 $R_\odot$, one sorar radius).

The Ratio $\frac{\text{Light}}{\text{Wind}} \approx$ const R^{-2} between 1 $R_\odot$ and 1 AU.

Future perspectives are mainly related with better and longer observations. The observed phenomena on the Sun are too complicated and theories are oversimplified, as a rule.

Currently:

ACE, Wind, SOHO, Yohkoh, Interball, Ulysses, Voyager 1 & 2, Pioneer 11 & 10 and others.

In the future:

STEREO (2003)
Solar Probe (under study)
Solar B (2003)
HESSI - High Energy Solar Spectroscopic Imager (2000)
Coronas F

Several illustrations are presented below from different sources.

K. Kiepenheuer. The Sun. The University of Michigan Press, Ann Arbor. 1959
First published as: Die Sonne, 1957, Springer-Verlag. Berlin

The solar atmosphere is known almost as intimately as our own. Unfortunately, conditions on the sun are such that we cannot simply apply our own meteorological findings to it. Because of the sun's high temperature, its different chemical composition, and the impossibility of simulating solar conditions in the laboratory, the solar physicist has to rely on theoretical physics and must avoid judging from terrestrial conditions.

Matters are much more difficult still when it comes to the sun's interior. Here we must rely on atomic theory, and our picture is always a reflection of our current knowledge of that theory and, like it, must constantly be modified. Solar physics and physics are therefore intimately related, and the serious reader would do well, if need be, to consult a popular textbook on physics.

In this book, you will get to know a star. The phenomena are so complex that the total picture of the sun may easily be lost sight of. I shall therefore begin with a bird's-eye view of solar astronomy to which the reader is advised to refer if ever he loses the thread of the argument.

Solar physics in 2000 words

The sun is one among a host of stars, that is, it is a gaseous body with a diameter of 864,000 miles and a mass of 2.10^{33} grams. Its distance from the earth is 93,000,000 miles, and light takes eight minutes to travel this distance. Under favorable conditions, the best solar telescopes reveal surface details down to a diameter of about 300 miles. Seen from the earth, the sun takes roughly four weeks to rotate on its axis. Strangely enough, it does not rotate like a solid body, for while the equator takes roughly 27 days to rotate, the polar regions take about 30 days. For thousands of millions of years, the sun's surface (which is at a temperature of about 10,800°F.) has been emitting 4.10^{23} kilowatts of energy per second in the form of light (electromagnetic

waves). The source of this energy lies deep within the sun, where the temperature is about 15,000,000°. Roughly 90 per cent of the energy comes from the region 0–0.23 r (r = radius of sun), where the density is 100 grams per cubic centimeter. This region represents 40 per cent of the total mass of the sun (Fig. 1). The energy is derived from the transmutation of hydrogen into helium, one gram of hydrogen supplying roughly 200,000 kilowatt hours.

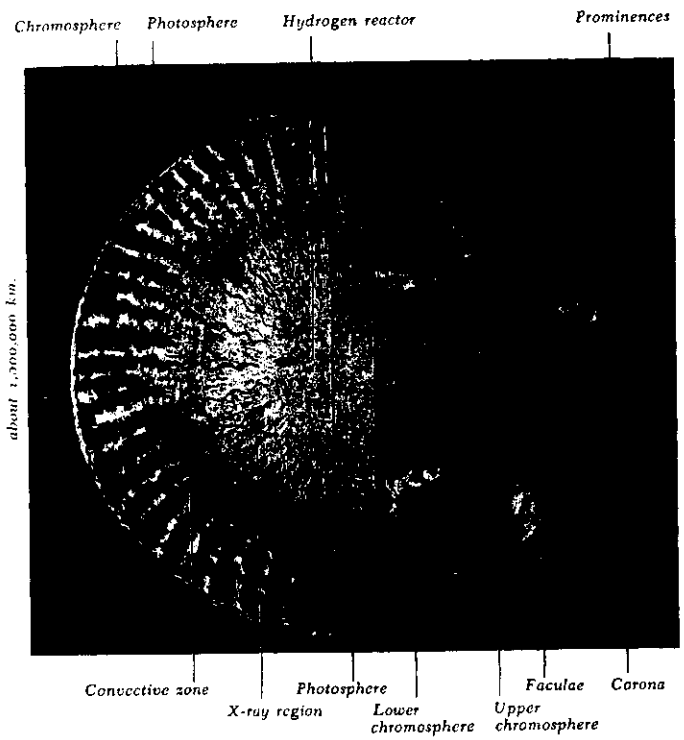

FIG. 1. Model of the sun. Right: The different layers composed from photographs. Left: Section through the sun.

This energy is broadcast outward in the form of X and γ rays in such a way that an equal quantity of energy flows through every concentric shell drawn about the center of the sun. If we draw a shell at a distance 0.7 *r* from the center, conditions have become such (temperature: 234,000°F.; density: 0.07 grams per cubic centimeter) that radiation alone can no longer maintain this flow of energy. Like water boiling in a kettle, the solar matter begins to seethe and carries its own heat to the surface. The area between 0.7 and 1.0 *r* is therefore known as the convective zone. Within this zone the density drops until it reaches 10^{-8} grams per cubic centimeter at the surface, and the temperature falls to about 9000°F.

At the surface the boiling mass assumes the shape of granules (irregular convection cells), each with a diameter of about 600 miles, and with an internal flow at the rate of about one mile a second. This upper layer is called the *photosphere*. For us it is the source of all sunlight.

Some 6000 miles above the photosphere, the density has rapidly decreased from 10^{-8} grams per cm^3 to 10^{-11} grams per cm^3, and to 10^{-16} grams per cm^3 some 12,000 miles higher up (the atmospheric density at the surface of the earth is $\approx 10^{-3}$ grams per cm^3). The light reaching us from these higher, rarefied strata is consequently so weak that it can only be observed with instruments which eliminate the glare of the photosphere.

Immediately above the photosphere lies the *chromosphere* or "color sphere." It has a depth of up to 6000 miles and, more turbulent than the photosphere, it is a constantly seething mass of gases. We may call the upper chromosphere the spray of the photosphere which—in a way not yet fully understood—is thrown up by the rising photospheric granules with velocities greater than six miles a second.

Unlike the terrestrial atmosphere, therefore, the chromosphere is not in static equilibrium. The temperature of this seething mass of froth and gaseous fountains is somewhat greater than the temperature of the photosphere.

At the outer edge of the chromosphere the density suddenly drops to 1/1000 the mean chromospheric density. Here, we find the *corona*, a gigantic layer of rarefied gases which stretches for millions of miles into space. The corona is directly visible only during total eclipses, when the moon hides the sun from view (Fig. 33). Its temperature is roughly 1,800,000°F.—much hotter than the chromosphere. In other words the kettle is hotter than the stove.

Even so, it would be wrong to imagine that the chromosphere heats the corona as a stove heats a kettle. What happens is that some kinetic energy escapes from the chromosphere into the corona by way of so-called shock-waves (supersonic pressure waves), and it is this kinetic energy which raises the temperature of the rarefied gases. In fact the temperature in the corona is so high that the coronal hydrogen nuclei (protons) completely lose their planetary electrons. Heavy nuclei such as carbon, nitrogen, and oxygen may lose up to 15 of their electrons.

The corona (which accounts for only 10^{-15} of the sun's total mass) is probably partly made up of interplanetary matter (dust and meteors). The constant gravitational pull of matter into the corona is probably balanced by constant solar evaporation into space.

The restless sun

The energy represented by the changes we shall now discuss is insignificant when compared with the radiation sent out by the sun. Changes in the appearance of the sun follow a rhythm of roughly 11 or 22 years, though the so-called solar cycle is not strictly periodic. The more striking changes occur mainly in certain

Amsterdam. 1972. PP. 306-316.

3. Plasma physics and its applications

efore we concentrate on our main topic: how the solar system originated, e should make a brief summary of the state of plasma physics. As you know, asma physics has started along two parallel lines. The first one was the ndred years old investigations in what was called electrical discharges in ses. This approach was to a high degree experimental and phenomenologi-l, and only very slowly reached some degree of theoretical sophistication. ost theoretical physicists locked down on this field, which was complicated d awkward. The plasma exhibited striations and double-layers, the electron stribution was non-Maxwellian, there were all sorts of oscillations and in-ibilities. In short, it was a field which was not at all suited for mathemati-lly elegant theories.

The other approach came from the highly developed kinetic theory of dinary gases. It was thought that with a limited amount of work this field uld be extended to include also ionized gases. The theories were mathemati-lly elegant and when drawing the consequences of them it was found that should be possible to produce a very hot plasma and confine it magnetically. nis was the starting point of thermonuclear research.

However, these theories had initially very little contact with experimental asma physics, and all the awkward and complicated phenomena which had en treated in the study of discharges in gases were simply neglected. The sult of this was what has been called the thermonuclear crisis some 10 years o. It taught us that plasma physics is a very difficult field, which can only developed by a close cooperation between theory and experiments. As S. W. Massey once said (in a somewhat different context): «The human ain alone is not able to work out the details and understanding of the inner orkings of natural processes. Without laboratory experiment there would no physical science today.»

The cosmical plasma physics of today is far less advanced than the thermo-clear research physics. It is to some extent the playground of theoreticians no have never seen a plasma in a laboratory. Many of them still believe in rmulae which we know from laboratory experiments to be wrong. The rophysical correspondence to the thermonuclear crisis has not yet come.

I think it is evident now that in certain respects the first approach to the ysics of cosmical plasmas has been a failure. It turns out that in several portant cases this approach has not given even a first approximation to th but led into dead-end streets from which we now have to turn back.

and origin of the solar system

The reason for this is that several of the basic concepts on which the theories are founded, are not applicable to the condition prevailing in cosmos. They are «generally accepted» by most theoreticians, they are developed with the most sophisticated mathematical methods and it is only the plasma itself which does not «understand» how beautiful the theories are and absolutely refuses to obey them. It is now obvious that we have to start a second approach from widely different starting points.

4. Characteristics of first and second approach to cosmic plasma physics

The two different approaches can be summarized in Table 1.

If you ask where the border goes between the first approach and the second approach today, an approximate answer is that it is given by the reach of spacecrafts. This means that in every region where it is possible to explore the state of the plasma by magnetometers, electric field probes and particle analyzers, we find that in spite of all their elegance, the first approach theories have very little to do with reality. It seems that the change from the first approach to the second approach is the astrophysical correspondence to the thermonuclear crisis.

Table 1

Cosmical electrodynamics

First approach	*Second approach*
Homogeneous models	Space plasmas have often a complicated inhomogeneous structure
Conductivity $\sigma = \infty$ Electric field $E_{\parallel} = 0$	σ depends on current and often suddenly becomes 0, $E_{\parallel}$ often $\neq 0$
Magnetic field lines are «frozen in» and «move» with the plasma.	Frozen-in picture often completely misleading.
Electromagnetic conditions illustrated by magnetic field line picture.	It is equally important to draw the current lines and discuss the electric circuit.
Electrostatic double layers neglected.	Electrostatic double layers are of decisive importance in low density plasmas.
Filamentary structures and current sheets neglected or treated inadequately.	Currents produce filaments or flow in thin sheets.
Theories mathematically elegant and very well developed.	Theories still not very well developed and partly phenomenological.

Enciclopedia of the Solar System. AIP. 1999

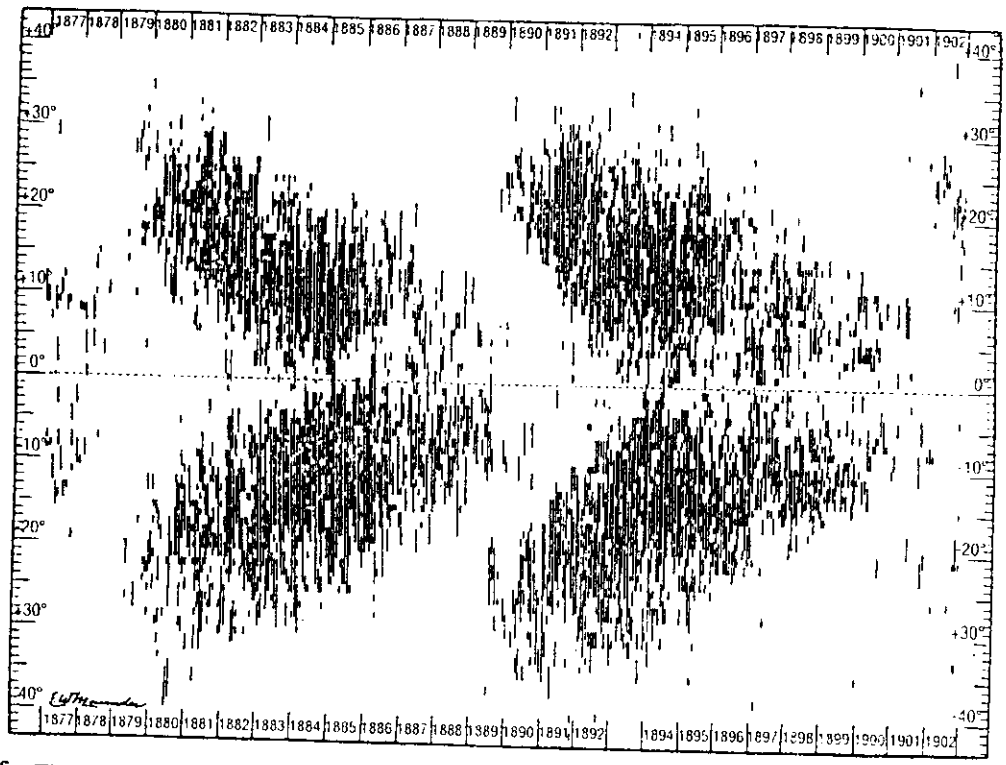

FIGURE 6 The "butterfly" diagram of the sunspot cycle. Spots of a new cycle appear at lower and lower latitudes. This is a copy of E. W. Maunder's discovery diagram, published in 1904. (Courtesy of *Monthly Notices of the Royal Astronomical Society.*)

Sound waves in the convection zone propagate at the local speed of sound, which increases with depth because the temperature increases. As a result, sound waves in the Sun are refracted as well as reflected. A plane wave that descends into the Sun at an oblique angle experiences a faster speed of sound at its deeper edge. Thus this edge gains over the shallower edge, and the plane wave turns back (refracts) toward the surface. Such a wave will trace a series of arcs, reflecting at the surface and refracting below it. If its horizontal wavelength is a simple fraction of the solar circumference, the wave is resonant and can persist as a standing wave. In general, waves of lower frequency (periods around 6 min) penetrate more deeply into the interior than waves of higher frequency.

Solar physicists derive the sound speed inside the Sun in much the same way that seismologists determine the sound speed inside the Earth. Whereas seismologists observe many transient earthquakes, solar physicists observe surface oscillations at many places on the photosphere and for many 5-min periods. The spatial distribution of the solar oscillations is fitted with mathematical functions (spherical harmonics) that assign the three quantum numbers (n, l, and m) to each observed mode. The temporal fluctuations of the velocity signal are Fourier-analyzed to derive the exact frequency of every resolvable mode. These primary data are then compared with the predicted frequencies from a standard model of the interior and the comparison yields corrections to the model's radial temperature distribution. As longer and longer series of continuous observations become available, the modes' frequencies are established with a precision of better than one part in a billion.

2. Detection Schemes

In their quest for high-frecuency precision, solar astronomers have resorted to a number of techniques. Precision ultimately depends on the length of a continuous time series of observations, uninterrupted even by the day–night cycle. These conditions can be met at the South Pole during the austral summer, subject only to occasional periods of bad weather. Several

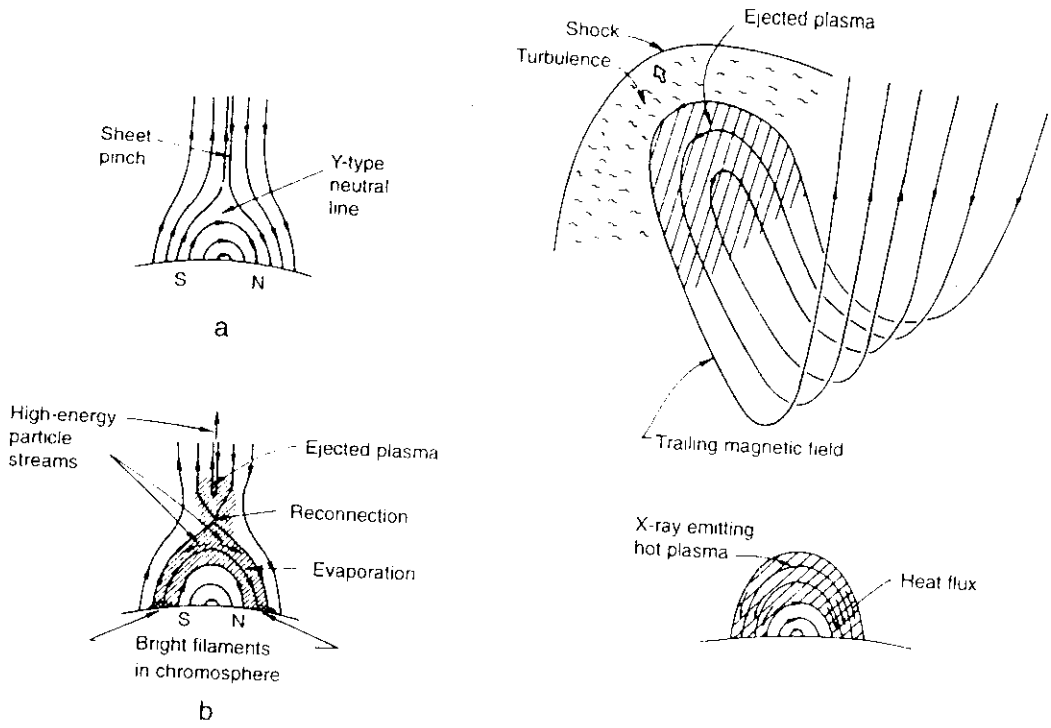

FIGURE 20 A diagrammatic sequence of the stages of a flare: (a) the preflare magnetic configuration, (b) the flash phase, (c) the thermal phase, following reconnection and ejection of hot plasma. (Courtesy of P. Sturrock, Colorado Associated University Press.)

region. The more complex the magnetic configuration of the region and the more rapidly new flux appears, the more likely a flare will occur. The simplest magnetic system that produces flares is a twisted magnetic loop that connects opposite magnetic polarity areas of the active region. A sunspot with opposite polarities within the same penumbra (a "delta" configuration) is especially prone to flaring.

The Japanese satellite *Yohkoh*, launched in August 1991, produced a vast quantity of high-quality observations of flares that are still being analyzed. These data are confirming many of the ideas developed since the flight of the *Solar Maximum Mission* (1980–1989), as well as revealing some surprises.

Although no single flare exhibits the full variety of flare phenomena, we shall attempt to describe the evolution of such a hypothetical flare, simply to give the reader an impression of the total event. The evolution of this ideal flare is illustrated schematically in Fig. 20. We can distinguish four phases: the preflare phase, the flash or impulsive phase, the thermal or gradual phase, and the postflare phase.

a. The Preflare Phase

In the preflare phase, which may last for minutes or tens of minutes, the active region shows signs of progressive heating. The brightness of many small sites increases and the region shows rapid fluctuations in H alpha, soft X rays, and microwaves. A filament that lies over the magnetic neutral line may be "activated," that is, may experience rapid changes in brightness and form, and may actually erupt just before the onset of the flare. Velocity oscillations have also been reported just before a flare.

Preceding the preflare phase is a long period in which magnetic flux continues to emerge and the field configuration is thought to become more sheared and twisted. One of the outstanding questions, still unanswered, is the conditions under which a flare is triggered.

b. The Flash Phase

The primary release of magnetic energy occurs in the low corona during the flash phase. The onset of the flare is marked by short pulses of hard X rays (photons

most ejections do not involve flares, but only the eruption of an unstable filament.

d. The Postflare Phase

Gradually, the flare plasma cools and much of it falls back to the chromosphere, as the active region returns to its approximate preflare state. Presumably, the region's nonpotential magnetic field has been reduced, but no direct information exists on the final (or initial!) configuration.

This relaxation process is sometimes accompanied by the formation of postflare coronal loops visible in H alpha and in the forbidden coronal emission lines typical of 2 to 4 million kelvin (Fe XIV and Ca XV). Coronal plasma seems to cool suddenly within a loop and flow downward. Higher loops appear successively, as though some process is gradually draining the upper corona.

An active region may emit a broadband circularly polarized continuum at meter wavelengths for hours or days following a flare. This Type IV radiation is thought to be synchrotron emission from energetic electrons trapped within a huge magnetic bottle.

2. Flare Models and Flare Physics

An enormous effort has been invested by solar physicists in attempts to understand the complex flare event. At present, general agreement exists on the basic physics involved in each phase, but detailed models are still goals for the future. The most obscure aspects of the flare phenomenon are the energy buildup, the triggering mechanism, and the acceleration of nonthermal charged particles. These are difficult to explain because they involve complex plasma physics at unresolvable spatial scales and large-scale magnetic field systems that are as yet unobservable. The later phases, involving the expansion and cooling of the flare plasma, are well documented and therefore better understood.

According to present ideas, flare energy is stored in the form of electric current systems or, equivalently, as nonpotential components of the active region's magnetic field. This energy accumulates as the footpoints of the magnetic field are shuffled by photospheric convective motions. A simple arcade of parallel coronal loops becomes sheared, and the individual loops may be twisted or braided. All this distortion creates increasingly large electric current densities within the coronal plasma.

The triggering of the flare may be driven by the intrusion of an opposite polarity field or may arise spontaneously as the field is distorted. Eventually, a current-driven instability may arise at some location. Several candidates have been proposed, among them the Buneman, ion–cyclotron, and ion–sound instabilities. When such an instability takes place, the resistivity of the plasma can increase by orders of magnitude and this allows magnetic field reconnection, in which nonpotential field components are destroyed and their energy is converted to charged particle kinetic energy via strong electric fields. Needless to say, this process is complicated and not well understood. To release a large flare energy, a large volume of magnetic flux must enter the reconnection zone and this requires some kind of external driving pressure or a propagating disturbance. Figure 21 is a model of a flaring loop, derived from *Yohkoh* observations of the flare of January 13, 1992.

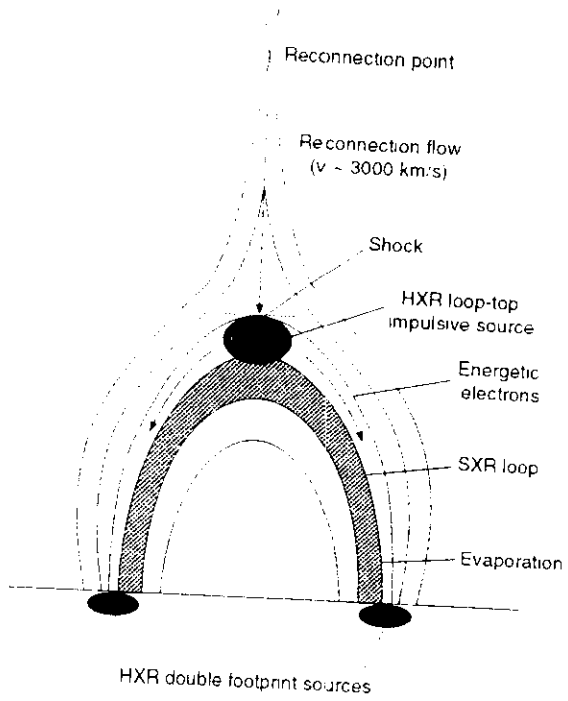

FIGURE 21 A model of a flaring loop, derived from *Yohkoh* observations. (Courtesy of the *Yohkoh* team.)

Once the beams of charged particles have been accelerated, their subsequent evolution is somewhat easier to describe. Fast electrons produce hard X rays as bremsstrahlung when they impact the dense plasma at the footpoints of coronal loops. The so-called "thick-

FIGURE 12 A magnetogram showing the strong and weak photospheric magnetic fields over the whole Sun during one 27-day rotation. Activity tends to concentrate in two bands at latitudes between 10° and 30°.

regularities are the so-called Hale–Nicholson laws (see Section IV).

As an active region decays (over a period of several months), differential rotation, meridian flow, and supergranule flows stretch out the region's flux into long bipolar regions at mid and high latitudes (see Fig. 2). As the bipolar field expands laterally and rises vertically, a helmet streamer (see Fig. 2) may develop in the overlying corona. As a result, the inner corona is reorganized into an array of streamers, separated by spokes of open field lines, which are called "coronal holes." X-ray images of the corona (see Fig. 3) show that in addition to these two basic structures, long coronal loops can connect different active complexes, even in different hemispheres.

Solar prominences form within a streamer, above a line in the photosphere that separates the opposite polarities of the weak bipolar region. They are flat sheets of plasma two orders of magnitude denser and cooler than the surrounding corona. Prominences appear as dark filaments on the solar disk, when photographed in the hydrogen H alpha line (Fig. 13).

Quiescent filaments, which lie outside of active complexes, possess horizontal magnetic field components that obey a global rule. In the northern hemisphere, the axial fields of such filaments are directed to the *right* when viewed by an imaginary observer who stands in the positive polarity region adjacent to the filament. Such filaments are called *dextral*. In the southern hemisphere, the axial field components are directed toward the *left* when viewed from the neighboring positive polarity region. Such filaments are called *sinistral*. Most filaments in the northern hemisphere are dextral, most in the southern hemisphere are sinistral, and this regularity does not change from one 11-year solar cycle to the next, despite the change in polarities of the leading sunspots.

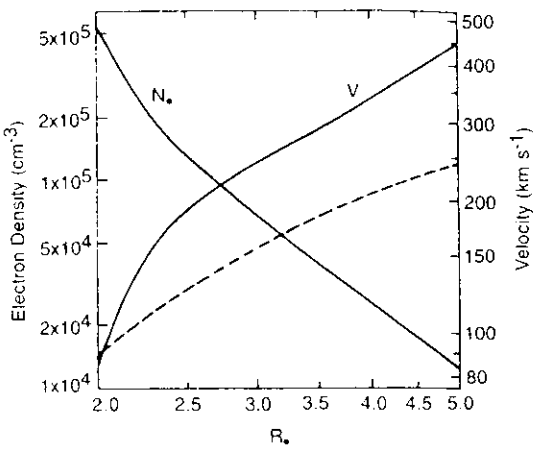

FIGURE 18 The radial variation of the electron density and flow speed in a coronal hole. The dashed line is the Parker wind solution for a coronal temperature of two million degrees kelvin. (Courtesy of *Astrophysical Journal*.)

form of the kinetic and gravitational energy of its wind stream. This large rate of energy loss poses a difficult theoretical problem, since E. N. Parker's classic explanation for the solar wind would require a coronal temperature of at least 2.5–3 million kelvin, whereas the holes have peak temperatures as low as 1.4 million kelvin. Somehow, energy or momentum must be deposited in the wind stream at radial distances of a few solar radii. Theorists have suggested that some form of hydromagnetic wave that propagates outward along the open field lines is responsible. Since Alfvén waves are detected in the wind near the Earth, they are considered prime candidates, but many problems arise concerning the production and dissipation of such waves. A complete understanding of the energetics of coronal holes and the wind within them remains for the future.

The size and location of coronal holes vary with the solar cycle. A few years before solar minimum, the poles of the Sun are covered by large coronal holes that occupy some 15% of their area. Occasionally the holes extend from a pole across the solar equator. Near solar maximum, the polar holes shrink in size, and smaller holes appear nearer the solar equator.

Like the rest of the corona, the holes rotate more rigidly (with periods of 26 to 29 days, independent of latitude) than the photosphere. Simulations of evolution of the coronal magnetic field, by Y. Wang and colleagues at the Naval Research Laboratory, suggest that this effect arises from transport of photospheric flux to higher latitudes and from reconnections of the coronal field.

IV. SOLAR ACTIVITY

Structures on the Sun change on timescales ranging from a few seconds to several months and their patterns evolve over a cycle of 22 years. We shall first discuss the solar magnetic cycle and then the more rapid transient events.

A. THE SUNSPOT CYCLE

1. Observations

The number and distribution of sunspots vary in a cycle of 8 to 13 years. At the beginning of the cycle, bipolar pairs of spots appear at latitudes above 60°. Then, as the cycle advances, increasing numbers of new spots appear at lower and lower latitudes. Thus, the latitude distribution of spots as a function of time mimics that of a butterfly's wings (see Fig. 6).

During a cycle, the magnetic polarity of all the leader (westernmost) spots in the northern solar hemisphere is the same, and is opposite to that of leader spots in the southern hemisphere. The polarity of leader spots reverses in each hemisphere at the beginning of the next cycle. Thus, the full magnetic cycle takes an average of 22 years. The leader spots of a new cycle possess the same polarity as the premaximum polar field of their hemisphere.

Similarly, the weak polar fields (2–10 G) reverse polarity close to the phase of sunspot maximum. However, oddly enough, the reversal at the two poles need not occur simultaneously! For example, the Sun possessed two negative poles during 1980.

The maximum number of sunspots in a cycle fluctuates by as much as a factor of two and this amplitude also seems to possess cycles, such as the 90-year Gleissberg cycle. In addition, periods of suppressed or negligible sunspot number have occurred during the past 7000 years, such as the Maunder minimum from 1645 to 1715. The Maunder minimum was accompanied by extraordinarily low temperatures throughout Europe and this correlation is perhaps the most convincing example of a solar influence on terrestrial weather.

As might be expected, the total magnetic flux in the photosphere varies with the 11-year cycle, by as much as a factor of five. During a cycle, the flux is constantly redistributed in latitude, from the intense concentrations in active regions to weaker large-scale regions at higher latitudes. Differential rotation, meridional flows, and supergranular flows combine to form the

From a study of ionic comet tails in the early 1950s, L. Biermann concluded that there must be a continuous outflow of charged particles from the Sun. He based this conclusion on calculations that indicated that the orientations of ionic comet tails, which always point away from the Sun independent of the orbital inclination of the comets, could only be explained in terms of an interaction between material emitted from the comets and charged particles continuously flowing outward away from the Sun into interplanetary space. Biermann estimated that a continuous particle flux on the order of 10^{10} protons cm^{-2} s^{-1} was needed at 1 AU to explain the comet tail observations. He later revised his estimate downward to a value of $\sim 10^{9}$ protons cm^{-2} s^{-1}. (Direct measurements by spacecraft show that the average solar wind particle flux at 1 AU is actually 3×10^{8} protons cm^{-2} s^{-1}.) [*See* PHYSICS AND CHEMISTRY OF COMETS.]

B. PARKER'S MODEL OF THE SOLAR WIND

Apparently inspired by these diverse observations and interpretations, E. Parker, in 1958, formulated a radically new theoretical model of the solar corona that proposed that the solar atmosphere is continually expanding into interplanetary space. Prior to Parker's work, most theories of the solar atmosphere treated the corona as static and gravitationally bound to the Sun. S. Chapman had constructed a model of a static solar corona in which heat transport was dominated by the thermal conduction of electrons. For a 10^{6} K coronal temperature, the classic electron thermal conductivity is 8×10^{5} ergs cm^{-1} s^{-1} deg^{-1}, and Chapman found that even a static solar corona must extend far out into interplanetary space. At the orbit of Earth, his model gave electron densities of 10^{2} to 10^{3} cm^{-3} and temperatures of $\sim 2 \times 10^{5}$ K. Parker realized, however, that such a static model leads to pressures at very large distances from the Sun that are seven to eight orders of magnitude larger than estimated pressures of the interstellar plasma. Because of this mismatch in pressures at large heliocentric distances, he reasoned that the solar corona could not be in hydrostatic equilibrium and must therefore be expanding. His consideration of the hydrodynamic (i.e., fluid) equations for mass, momentum, and energy conservation for a hot solar corona led him to unique solutions for the coronal expansion that depended on the value of the coronal temperature close to the surface of the Sun. The expansion produced low flow speeds close to the Sun, supersonic flow speeds (i.e., flow speeds greater than the speed with which sound waves propagate) far from the Sun (Fig. 1), and vanishingly small pressures at large heliocentric distances. In view of the fluid character of the solutions, Parker called this continuous, supersonic, coronal expansion the "solar wind."

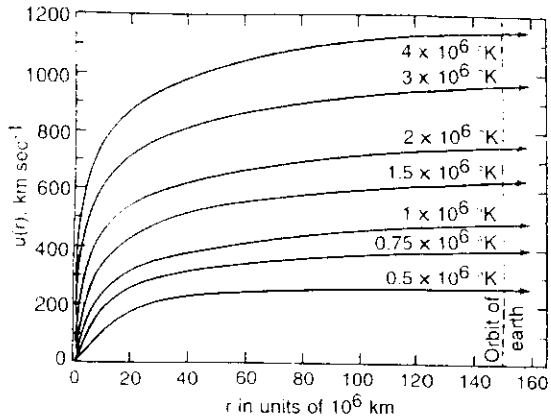

FIGURE 1 E. N. Parker's original solutions for solar wind flow speed as a function of heliocentric distance for different coronal temperatures. Subsequent work has demonstrated that the simple relationship between coronal temperature and solar wind speed illustrated here is incorrect. [From E. N. Parker (1963). "Interplanetary Dynamical Processes." Interscience, New York. Copyright © 1963. Reprinted with permission of John Wiley & Sons, Inc.]

C. FIRST DIRECT OBSERVATIONS OF THE SOLAR WIND

Parker's theoretical ideas about the solar wind originally met with some resistance, but experimental confirmation was not long in coming. Several early Russian and American space probes in the 1959–1961 era penetrated interplanetary space and found tentative evidence for a solar wind. Firm proof was provided by C. Snyder and M. Neugebauer, who flew a plasma experiment on the *Mariner 2* space probe on its epic 3-month journey to Venus in late 1962. Their experiment detected a continual outflow of plasma from the Sun that was highly variable, being structured into alternating streams of high- and low-speed flows that lasted for several days each. Several of the high-speed streams apparently recurred at the rotation period of the Sun. Average solar wind proton densities (normalized for a 1 AU heliocentric distance), flow speeds, and temperatures during this 3-month interval were 5.4 cm^{-3}, 504 km s^{-1}, and 1.7×10^{5} K, respectively, in essential agreement with the predictions of Parker's model. The *Mariner 2* observations also showed that helium, in the form of alpha particles, is present in

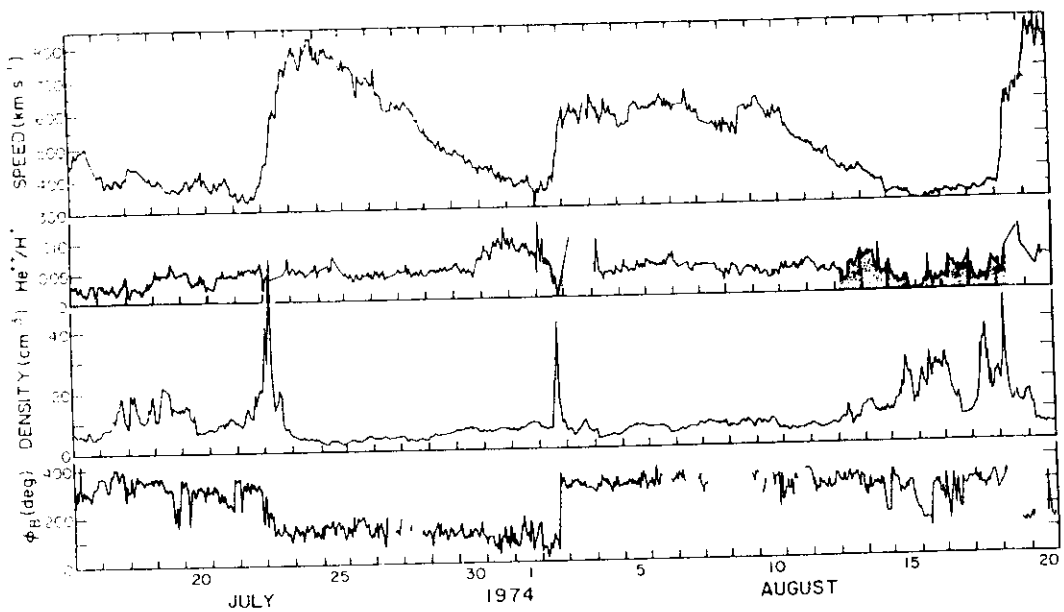

FIGURE 4 Selected solar wind parameters for a 36-day interval in 1974, illustrating characteristics of solar wind stream structure as observed near Earth's orbit. [From J. T. Gosling *et al.* (1981). *J. Geophys. Res.* **86**, 5438.]

C. THE CONNECTION BETWEEN CORONA STRUCTURE AND SOLAR WIND STREAM STRUCTURE

Figure 5 provides a schematic illustration of the connection between solar wind stream structure and coronal structure. Quasi-stationary high-speed streams originate in coronal holes (the dark regions in Fig. 3), which are large, nearly unipolar regions in the solar atmosphere. The coronal density is relatively low within coronal holes because the solar wind expansion there is relatively unconstrained by the solar magnetic

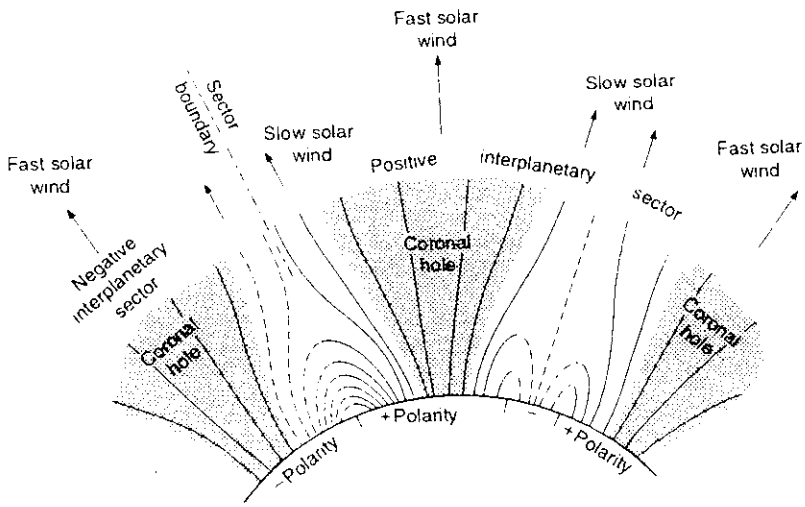

FIGURE 5 Schematic illustrating the relationship between coronal structure and solar wind stream structure. [From A. J. Hundhausen in "Coronal Holes and High Speed Wind Streams" (J. B. Zirker, ed.). Reprinted with permission of Colorado Associated University Press.]

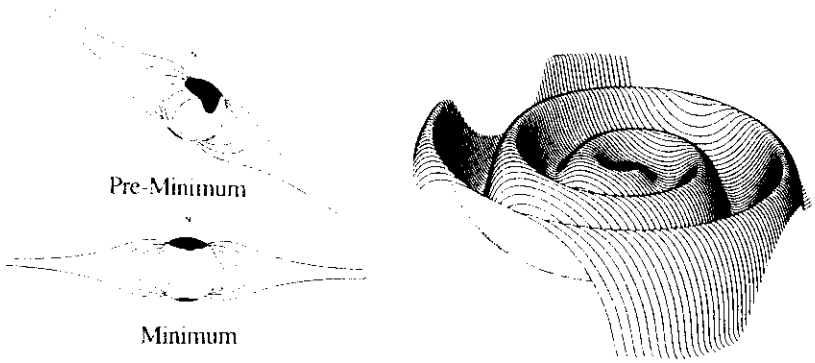

FIGURE 6 Right: schematic illustrating the configuration of the heliospheric current sheet in interplanetary space when the solar magnetic dipole is strongly tilted relative to the rotation axis of the Sun. The heliospheric current sheet separates interplanetary magnetic fields of opposite magnetic polarity and is the interplanetary extension of the solar magnetic equator. Left: schematic illustrating the changing tilt of coronal structure and the solar magnetic dipole relative to the rotation axis of the Sun as a function of phase of the solar activity cycle. Adapted from J. R. Jokipii and B. Thomas (1981). *Astrophys. J.* **243**, 1115, and from A. J. Hundhausen (1977). *In* "Coronal Holes and High Speed Wind Streams" (J. B. Zirker, ed.). Reprinted with permission of Colorado Associated University Press, Boulder.]

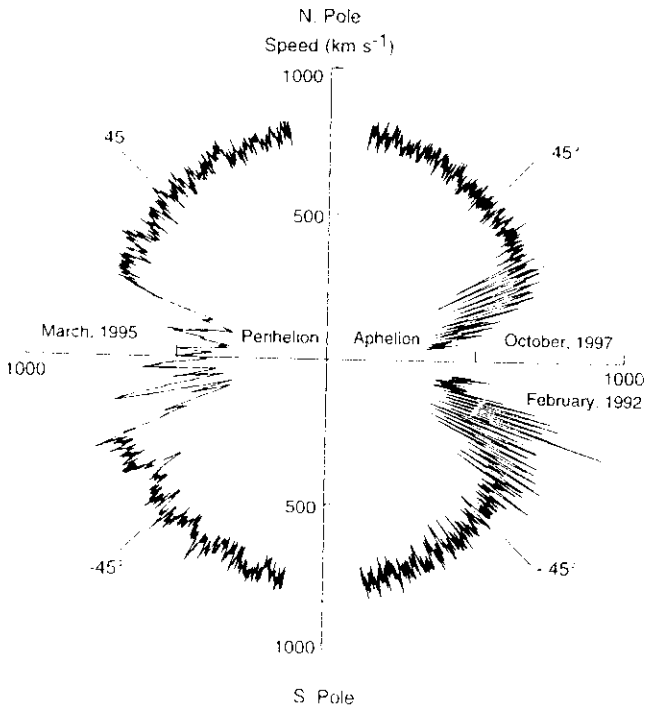

FIGURE 7 Solar wind speed as a function of heliographic latitude as measured by the *Ulysses* space probe from mid-February 1992 through mid-October 1997. Data shown in the left portion of the figure are centered on orbit perihelion at 1.4 AU, whereas data on the right are centered on orbit aphelion at 5.4 AU. The apparent difference in the latitude scale of structure in the flow speed in the left and right portions of the figure is an artifact associated with the fact that the spacecraft changed latitude very rapidly near perihelion but only very slowly near aphelion.

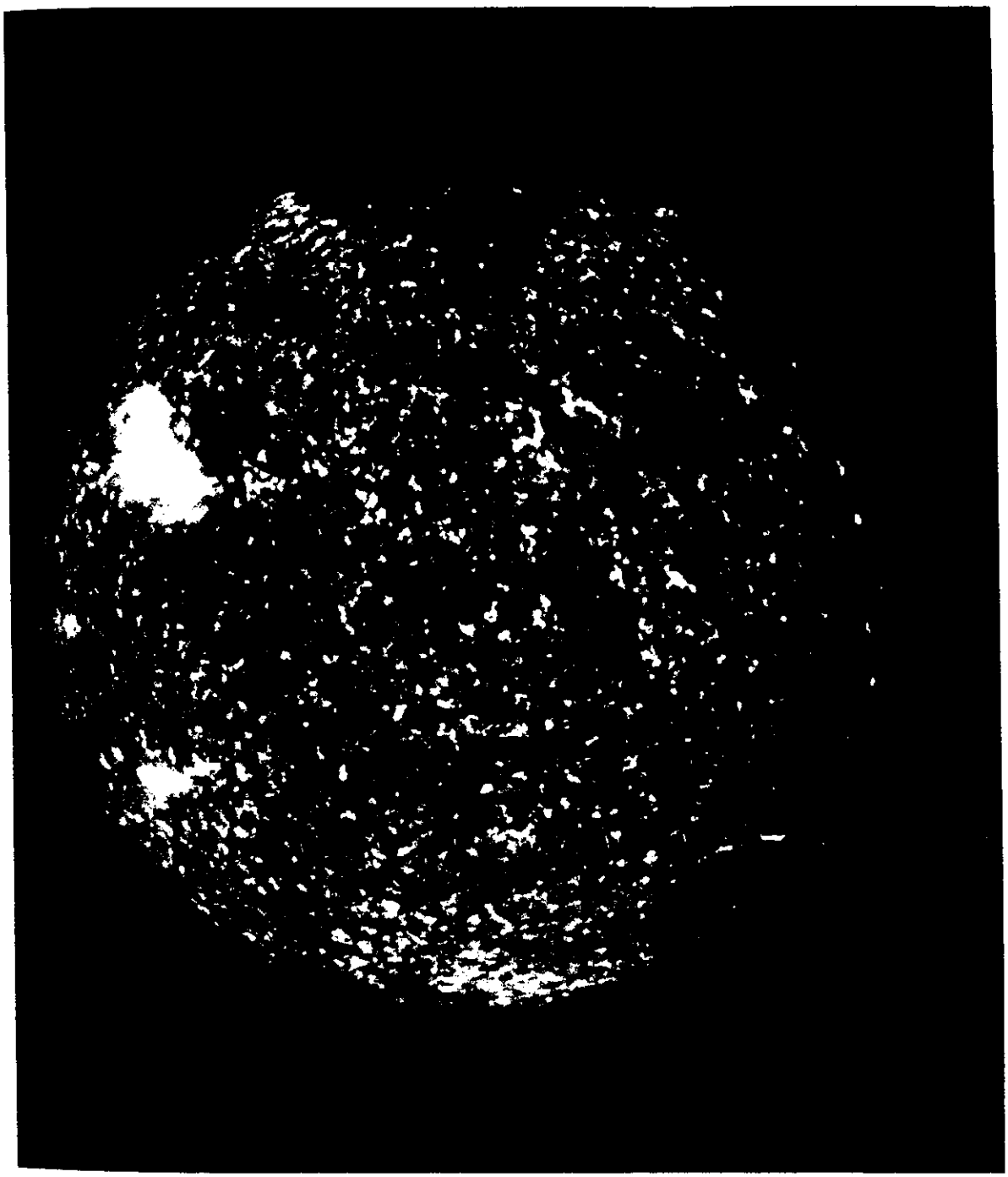

Sun-twisting magnetic fields propel this huge eruptive prominence about 150,000 km above the Sun's surface. The seething ionized gases is at a temperature of about 85,000 K and spans over 300,000 km. The space-based Solar Heliospheric and Oscillations SOHO recorded this image from its vantage point in a Halo orbit. (SOHO-EIT Consortium, ESA, NASA)

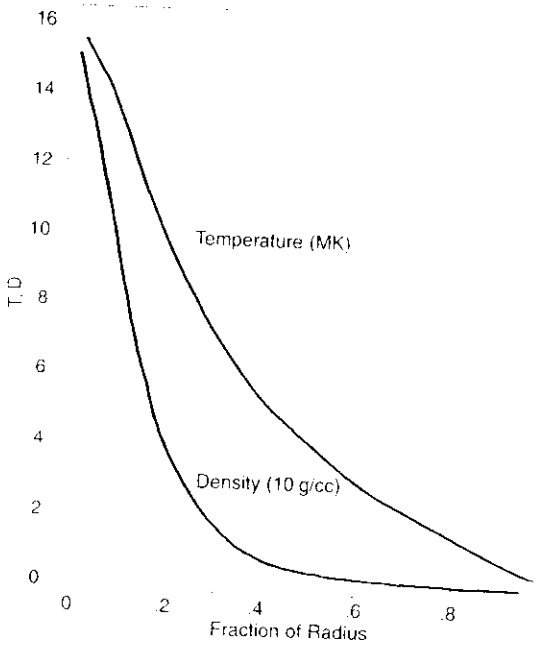

FIGURE 7 The radial variation of temperature and mass density in the solar interior as predicted by the "standard" solar model. The temperature scale is in millions of kelvin (MK) and the density scale is in tens of grams per cubic centimeter.

groups have observed the oscillations for as long as two weeks at the pole.

Alternatively, a network of observing stations has been used to observe the Sun continuously for several months. The Global Oscillation Network Group (GONG), a consortium of a hundred astronomers, is currently analyzing data from the most ambitious of these networks. GONG consists of six identical instruments distributed in longitude around the world. A map of photospheric velocities is obtained every minute from each site. These maps are collected every few weeks, calibrated at a center in Tucson, Arizona, and distributed to the consortium. GONG will operate continuously for at least three years to acquire perhaps the most complete set of observations attainable from Earth.

Finally, an oscillation detector is operating aboard the Solar and Heliospheric Observatory, a space mission launched in early 1996. The Sun is observable continuously from this spacecraft without any interference from weather or atmospheric scintillations, since it is located at the L1 Lagrangian point, a million kilometers from Earth in the direction of the Sun.

3. Some Results

The past decade of helioseismology, and especially the past year of GONG operation, has yielded several important results. We now know that helium nuclei represent about 24% of the mass of the interior, the heavy elements compose about 2.5%, and the remainder is hydrogen in the form of protons. Moreover, determinations of the sound speed along a radius yield the temperature profile of the interior. The agreement with theoretical models is very good.

Observations of the Sun's surface showed long ago that the solar equator rotates about 50% faster than the regions near the poles. Since the surface evidently does not rotate as a rigid body, how does the interior rotate? Helioseismology has provided an answer.

Sound waves propagate in a medium at a speed fixed by the temperature of the medium. If the medium itself is moving, the sound waves are carried along with it, and their observed speed is thus higher or lower depending on the wave's direction relative to the medium's direction. Thus, the observed frequencies of solar sound waves shift higher or lower, as a result of the Doppler effect, when the waves pass through layers that rotate at different speeds. Each original frequency is split into a pair that corresponds to waves traveling in the same or opposite direction as the rotation. Since short-period waves favor the surface and longer-period waves favor the deeper layers, it is possible to combine observations of rotational frequency splitting in such a way as to find the speed of rotation as a function of depth and latitude in the solar interior. Figure 9 illustrates some recent results. In the convection zone, rotation speeds tend to remain constant with depth, but vary with latitude. Just beneath the photospheric equator lies a belt of maximum speed. The radiative zone seems to rotate as a rigid body, somewhat slower than the equator at the surface.

4. Gravity Waves

Note that the derived rotation speeds are uncertain below the convection zone and missing entirely in the solar core, where few sound waves penetrate. Some astrophysicists expect that the Sun has a rapidly rotating core, a remnant of its original contraction from a gas cloud. To examine the deep interior, helioseismologists will have to study a different type of global oscillation, namely, gravity waves. In this type of oscillation, buoyancy, rather than pressure, supplies the restoring force. Gravity waves are predicted to have long periods (hours) and very small velocity amplitudes

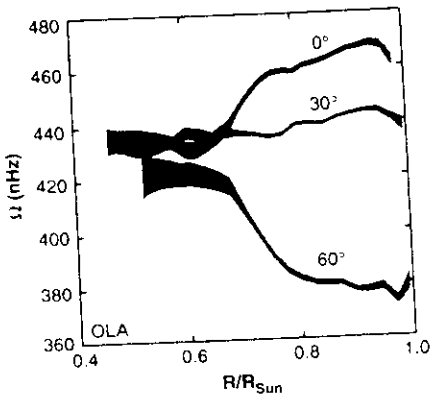

FIGURE 9 Rotation frequency as functions of radius and latitude, determined from helioseismic observations. (430 nHz corresponds to a rotation period of 27 days.) (Courtesy of *Science*.)

(millimeters per second). Since they are almost entirely confined to the deep interior, the detection of these oscillations will require very sensitive techniques. A number of researchers have claimed to detect gravity waves, but not convincingly. The study of these weak oscillations remains for the future.

5. Oscillations of Brightness

Global acoustic oscillations produce fluctuations in the brightness of the photosphere as well as of the next higher layer, the chromosphere. The lowest-degree oscillations, which correspond to the longest wavelengths, have been detected in the flux of integrated sunlight by active cavity radiometers aboard a series of satellites. NASA has attempted to place such detectors on every suitable satellite because of the potential importance of such measurements for the Earth's climate. The signal is only a few parts in a million of the steady solar output but is quite unambiguous.

6. The Future

The future successes of helioseismology are difficult to predict, but this new field of solar physics will undoubtedly play an important role in the investigation of the generation of solar magnetic fields. Studies of the solar cycle of magnetic activity will certainly benefit from helioseismic data. Moreover, astronomers are already attempting to find stellar analogs of solar oscillations, and indeed have found them in a class of white dwarfs.

III. THE SOLAR ATMOSPHERE

As Figs. 2 and 3 illustrate, the solar atmosphere is hardly a smooth, spherically symmetrical shell. Instead it consists of a complicated arrangement of interleaving structures that have spatial scales ranging from a few hundred kilometers to several hundred thousand kilometers. Each type of structure has its own characteristic temperature and density distribution. For a first crude description, however, it is useful to refer to several "layers," arranged along an outward radius, that correspond roughly to regions of increasing temperature and decreasing density. We have already referred to the names given to these layers: the photosphere, chromosphere, transition zone, and corona. In addition, one can distinguish between the active atmosphere, in the general vicinity of a sunspot group, and the quiet atmosphere, far from such a group.

A. THE SPECTRUM OF THE QUIET SUN

The solar spectrum is the source of much of our knowledge of the atmosphere. The photospheric continuum ("sunlight") has an approximate blackbody form with a color temperature of about 6000 K. Superposed on this continuum are the Fraunhofer absorption lines, which correspond to transitions in atoms of neutral and singly ionized metals, such as sodium, magnesium, and iron. The bands of many simple molecules, such as CO, CH, and CN, are also present in the spectrum. Over 20,000 atomic lines have been identified in the optical spectrum and their relative strengths, corrected for their atomic transition probabilities, yield the Sun's chemical composition. The relative concentrations of some of the more common elements are shown in List 2.

The optical spectrum of the chromosphere, originally observed at total eclipses at the limb of the Sun, is almost a "reversal" of the photospheric spectrum: each dark absorption line appears as a bright emission line. In addition, the chromosophere radiates strongly in the resonance lines of hydrogen, helium, magnesium, and other abundant elements, at wavelengths between 100 and 300 nm.

In the transition zone, the emission lines arise from multiply ionized abundant elements, such as C IV, N V, and O V. (C IV denotes the ion of carbon that has had three of its original electrons stripped off.) These lines appear mainly in the extreme ultraviolet, at wavelengths between 30 and 150 nm.

The spectrum of the nonflaring corona contains

resonance emission lines of highly ionized species, such as Fe IX to Fe XVI, at wavelengths between 10 and 50 nm. In addition, "forbidden" (quadrupole) transitions of ions such as Fe X, Fe XIV, and Ca XV appear in the optical coronal spectrum against a faint coronal continuum. The latter is produced by the scattering of photospheric light from free coronal electrons, and at radial distances beyond two solar radii, by scattering from interplanetary dust particles. [*See* INTERPLANETARY DUST AND THE ZODIACAL CLOUD.]

Solar flares produce the full range of plasma temperatures, from 10^4 to 10^7 K. The hottest regions briefly emit spectrum lines of such hydrogenlike ions as Ca XIX and Fe XXV.

The quiet Sun also emits a full spectrum of radio waves. The plasma density of the emitting region determines the characteristic wavelength. Thus the photosphere emits millimeter waves, the chromosphere emits centimeter waves, and the corona emits decimeter and meter waves. Active regions, sunspots, and flares emit polarized radio radiation with rapid time variations. [*See* THE SOLAR SYSTEM AT RADIO WAVELENGTHS.]

B. THE RADIAL TEMPERATURE AND DENSITY PROFILES

From the great number of spectroscopic observations collected over the past century, astronomers have constructed empirical one-dimensional models of temperature and density as functions of height through the atmosphere. Figure 10 shows averages for the quiet atmosphere. Note that the electron temperature passes through a minimum of about 4400 K, a few hundred kilometers above the visible surface and then rises steeply through the chromosphere and the transition zone to the million-degree corona. However, recent infrared observations of carbon monoxide molecules indicate that, over much of the solar surface where photospheric magnetic fields are weak, the temperature minimum is a mere 3000 K.

Except for the region near the temperature minimum, hydrogen is fully ionized. The atmosphere consists of a mixture of positive ions (principally protons) and electrons. It is electrically neutral and is called a "plasma." The radial distribution of ion number density at the poles differs from that at the equator.

The photosphere is sufficiently dense and opaque to ensure that thermodynamic equilibrium at the local temperature prevails in each volume. The spectrum of the radiation inside the photosphere resembles that of a blackbody and the ionization and excitation of the

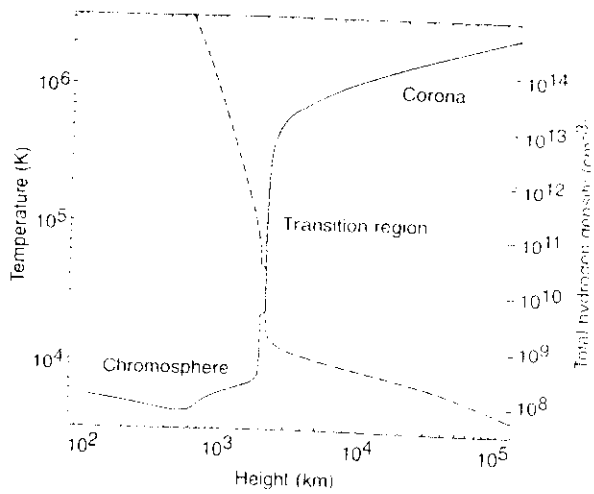

FIGURE 10 The variation with height of the temperature and proton density in a one-dimensional model of the solar atmosphere. (Courtesy of *Annual Reviews of Astronomy and Astrophysics*.)

elements are controlled by the Saha and Boltzmann laws, respectively. In the chromosphere, transition zone, and corona, the plasma is partially or wholly transparent to radiation, and collisions among particles are much less frequent. Therefore, thermodynamic equilibrium is not valid in these regions. A complex formalism, based on the assumption of a steady state of microscopic processes, has been developed over the past 30 years to analyze conditions in the more tenuous layers. The equilibrium ionization and excitation of the elements are governed by collisions among ions and electrons, at rates set by the local electron temperature and density. In this portion of the atmosphere, radiation is produced ultimately by collisions among particles and it emerges, without appreciable absorption, with a non-Planckian distribution.

C. THE ENERGY BALANCE OF THE ATMOSPHERE

According to current ideas, the steep rise in temperature through the atmosphere is the result of a balance between heating (by nonradiative energy that is generated in the convection zone) and cooling (by radiation to space). A comprehensive understanding of this energy balance and the resulting distribution of temperature and density has not been achieved as yet, but considerable progress has been made in studying the energy balance in individual layers.

At least three forms of nonradiative energy that heat the outer atmosphere have been suggested. Sound waves with periods between a few tens of seconds and a few hundred seconds can be generated as a by-product of turbulent convection below the photosphere. Waves with frequencies above a critical value (corresponding to about 300 s) can propagate vertically. As the waves rise into regions of rapidly decreasing density, their velocity amplitudes would increase accordingly, and when their amplitudes reached the local sound velocity, the waves would shock and dissipate their energy. The lower layers of the chromosphere are thought to be heated in this fashion. Propagating sound waves have been detected and studied by various means; their existence is well established.

Magnetohydrodynamic (MHD) waves, particularly Alfvén waves, have been suggested as agents for heating the upper chromosphere and corona. However, Alfvén waves are difficult to generate with the slow convective motions and, moreover, Alfvén waves do not dissipate readily. The best empirical evidence for the possible existence of such hydromagnetic waves in the atmosphere is the nonthermal broadening of spectrum lines in the low corona. The width of such lines is fixed in part by the distribution of thermal speeds of the radiating ions. However, observations show that the line widths are larger than simple thermal broadening can explain. The excess width has been attributed to excess nonthermal motions, among them MHD waves.

If sound waves shock in the chromosphere and if the evidence for MHD waves is weak, how is the million-degree corona heated? In recent years, E. N. Parker at the University of Chicago has argued effectively for heating by ohmic dissipation of electrical currents. He proposes that the currents arise from the slow twisting and braiding of coronal magnetic fields as the footpoints of the fields are shuffled by convective motions in and below the photosphere. The currents would be confined to extremely thin sheets (as narrow as 30 m) at places in the corona where the field direction changes discontinuously. As the convective motions continue to deform the coronal field, the current density rises in the sheets. Eventually they become unstable to a variety of plasma instabilities and dissipate, converting their electrical energy to heat and mass motions. During this process, magnetic fields with oppositely directed components can reconnect and release a fraction of their nonpotential energy. Such dissipative processes have been observed in Tokamaks and in three-dimensional numerical simulations, and are postulated to occur in flares (see Section IV). The result of such field reconnection in the corona should be a tiny flare, a "nanoflare," that emits a burst of X rays and radio radiation. The corona would be heated, in Parker's scheme, by many small episodic injections of magnetic energy. To supply the corona's energy requirements, such nanoflares would have to occur in sufficient numbers. Counts of very small flares, observed with the *Yohkoh* satellite, fail to meet this criterion. The long-standing problem of coronal heating remains unsolved at the present time.

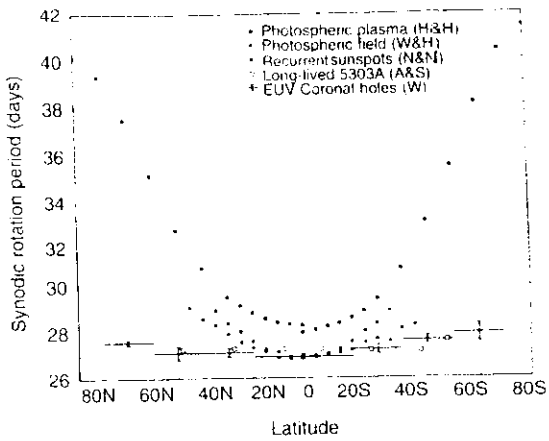

FIGURE 11 The rotation period of different parts of the Sun. The equator rotates faster than the poles and the corona rotates more rigidly than the photosphere. (Courtesy of Colorado Associated University Press.)

D. LARGE-SCALE MOTIONS

The rotation of the photosphere has been determined from daily maps of Doppler velocities (principally at the Mount Wilson Observatory) or from the displacements of individual features, such as sunspots or magnetic field patches. Although different methods yield slightly different results, the general features persist. The visible photosphere rotates from east to west but not as a rigid body would. Instead the equator rotates faster (in 25 days, relative to the distant stars) than the higher latitudes. At latitudes of $\pm 75°$, for example, the photosphere rotates in 34 days. This latitude-dependent effect is called the differential rotation (Fig. 11). The photosphere also flows slowly from the equator to the poles, at a speed of about 10 to 20 m/s.

As Fig. 11 shows, the corona (whose brightness is dominated by coronal streamers) tends to rotate more rigidly than the photosphere, but the details are complicated. A recent analysis of white light images shows

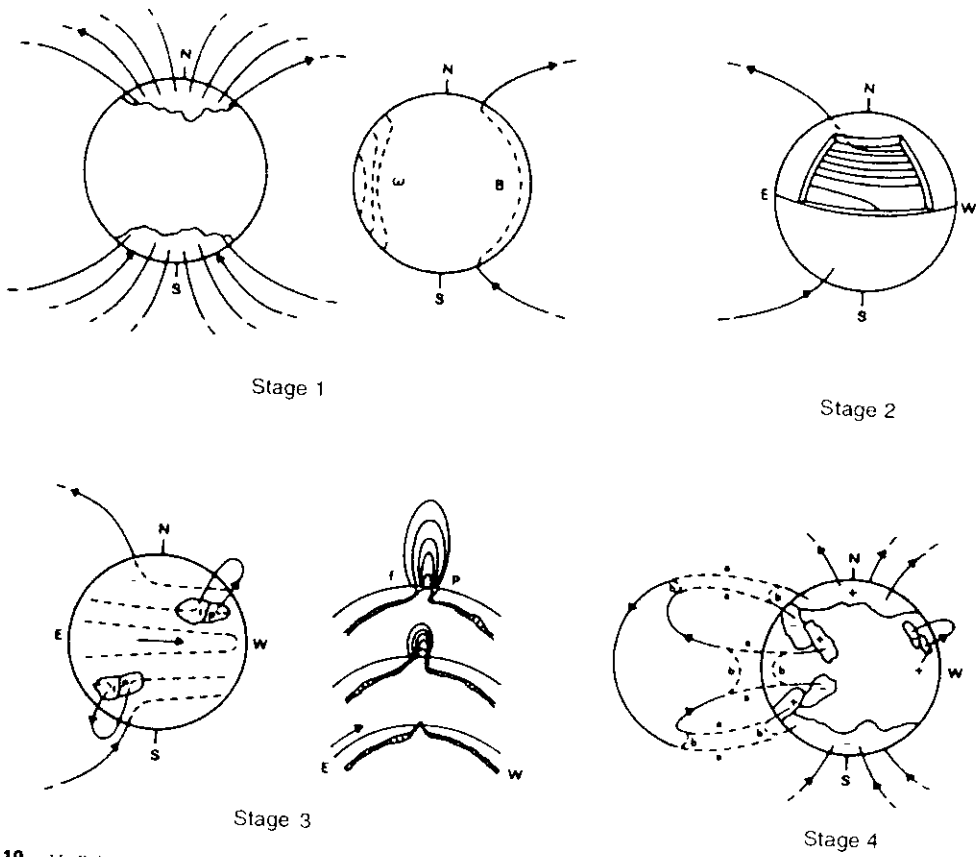

FIGURE 19 H. Babcock's conceptual model of the solar cycle. See the text for a description. (Courtesy of *Astrophysical Journal*.)

the zone. Models based on this idea and incorporating plausible physics do seem capable of maintaining the solar magnetic flux, but still have difficulties in transporting the amplified field to the surface.

B. SOLAR FLARES

1. Observations

A solar flare appears as sudden brightening of part of an active region (see Fig. 5). The region is heated to tens of millions kelvin, often within a few minutes, and may emit radiation over the full electromagnetic spectrum from gamma rays to long radio waves. In addition, beams of nonthermal electrons and protons can be accelerated to millions of electron volts and, along with masses of hot coronal gas, can be ejected into interplanetary space. The total energy of a large flare (10^{31} ergs) is sufficient to power the entire United States for a hundred thousand years.

Some of this radiation and particle emission reaches the Earth and produces a variety of effects, including electric power grid surges, radio propagation anomalies, and auroras. In March, 1989, the entire electric power grid of eastern Canada was shut down by a powerful series of solar flares. Thus, flare research has a practical as well as an astrophysical aspect.

Since flares occur in active regions, their frequency follows the 11-year solar cycle. At sunspot maximum, scores of small flares and several large ones occur daily. The frequency with which flares occur, as a function of energy, is a power law with an index of -1.8. This means that flares with half the energy of another group of flares will occur about four times more often, on average. Flares last anywhere from a few minutes to many hours, usually depending on their area and total energy.

In general, flares tend to occur near the boundary between the opposite magnetic polarities of an active

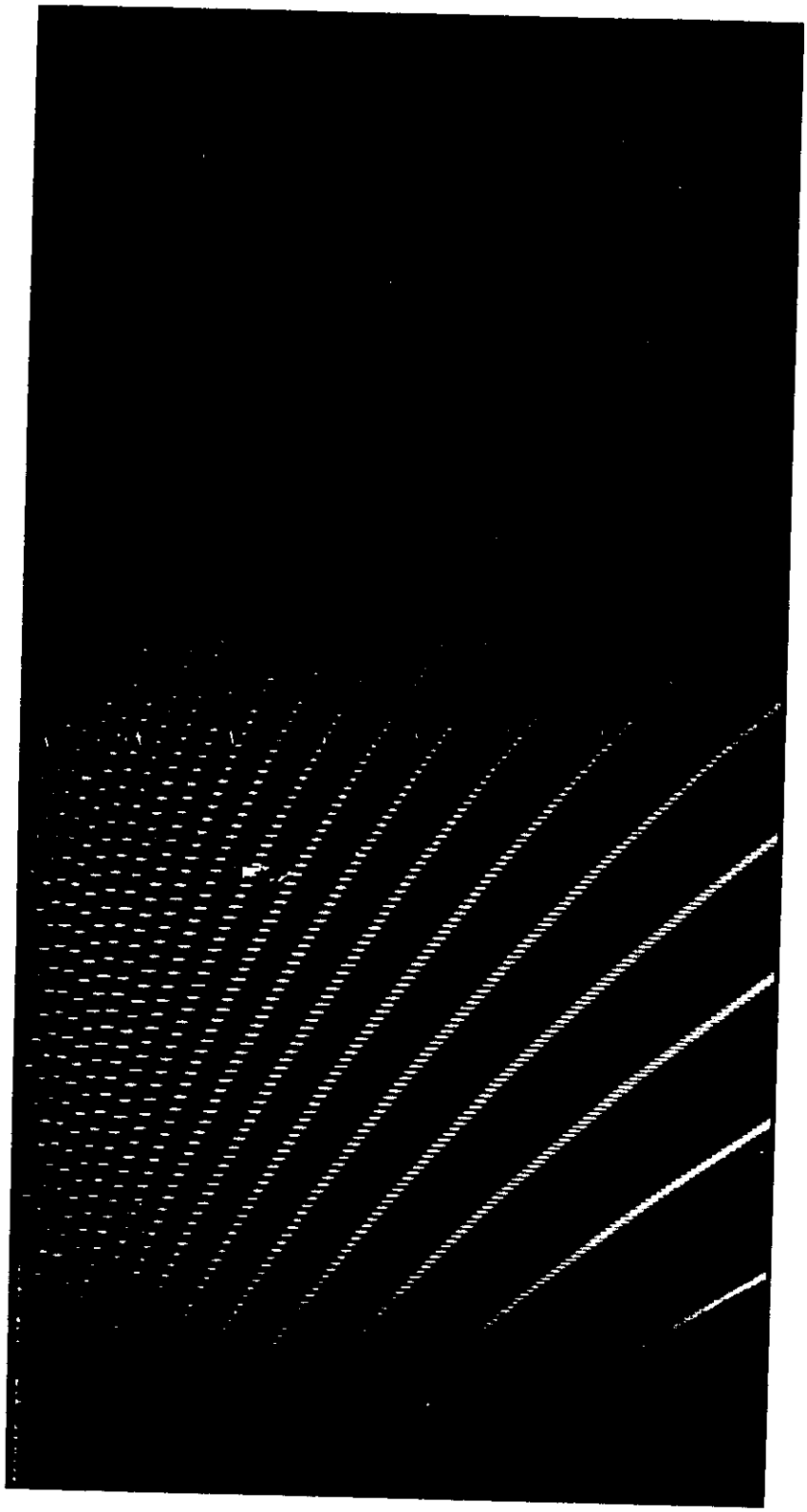

FIGURE 8 The acoustic power present in global oscillations, as functions of inverse wavelength (horizontal axis) and frequency (vertical axis). Each ridge is a family of modes that have a definite number of radial modes, the $n = 1$ mode lying lowest and farther to the right in the diagram. Each ridge is further subdivided (the small dashes) into modes with different numbers of meridional modes.

Solar wind — LISM

Local Interstellar Medium

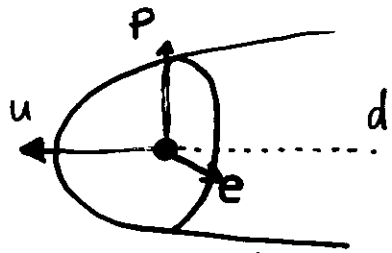

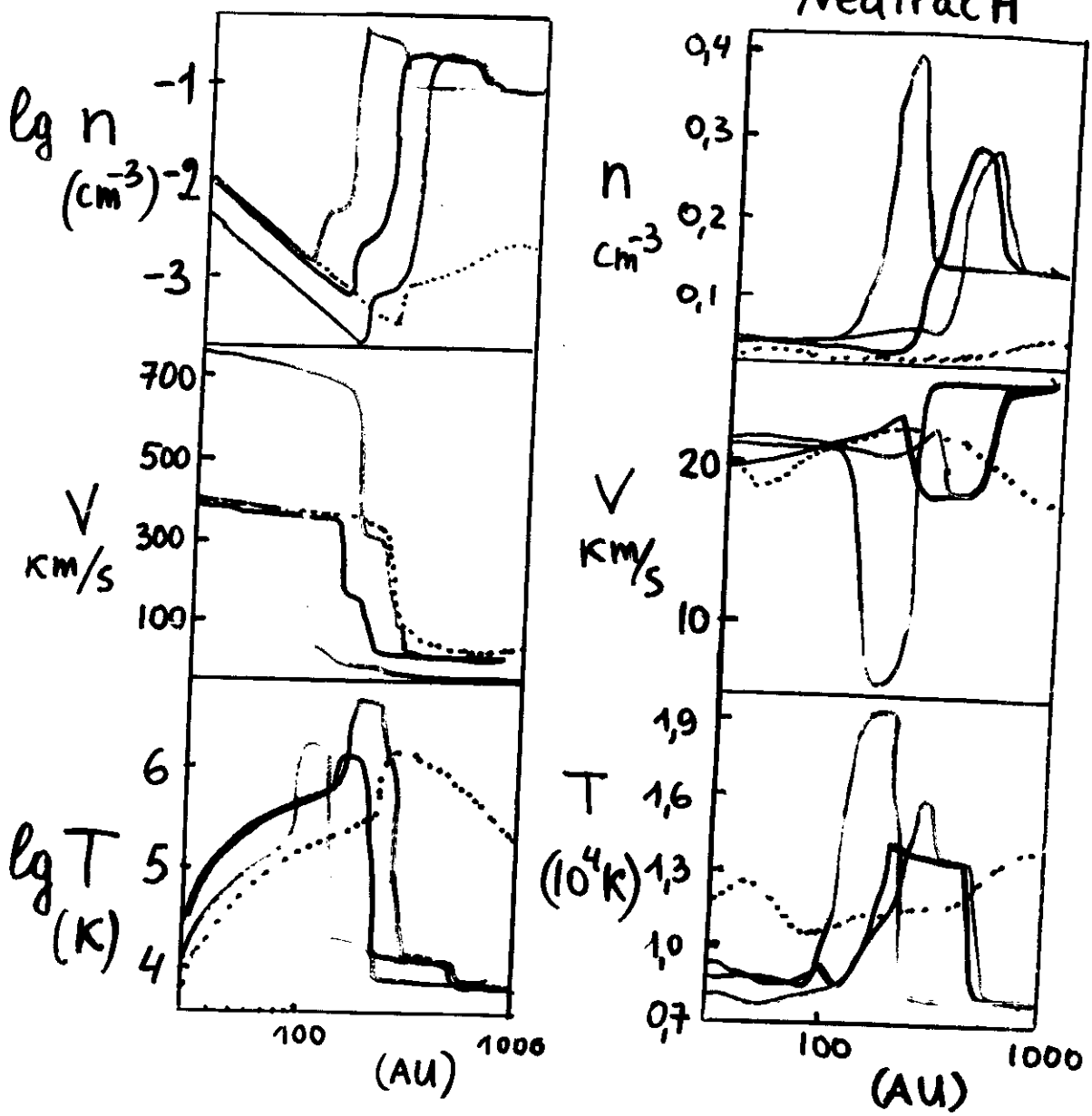

T. Gombosi (1998)

G. Zank et al. (1996, 1997)

V.B. Baranov et al. (1999)

MHD

multifluid HD

Monte Carlo

Moving radiation belts in the heliosphere

Luminating barrier:
$t = 0$: $B_i r_i = max.$

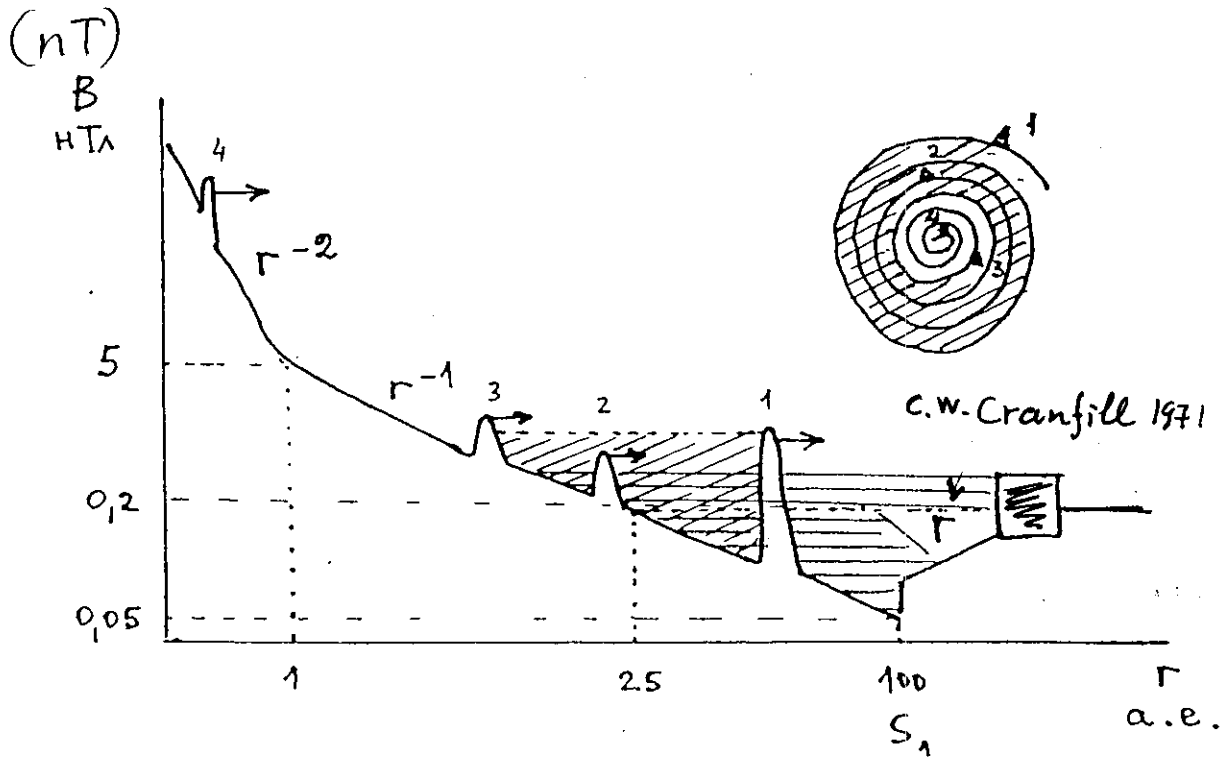

A ((

Magnetic wall
Washimi H., Tanaka T. 1996

JGR 103, A6, 1998

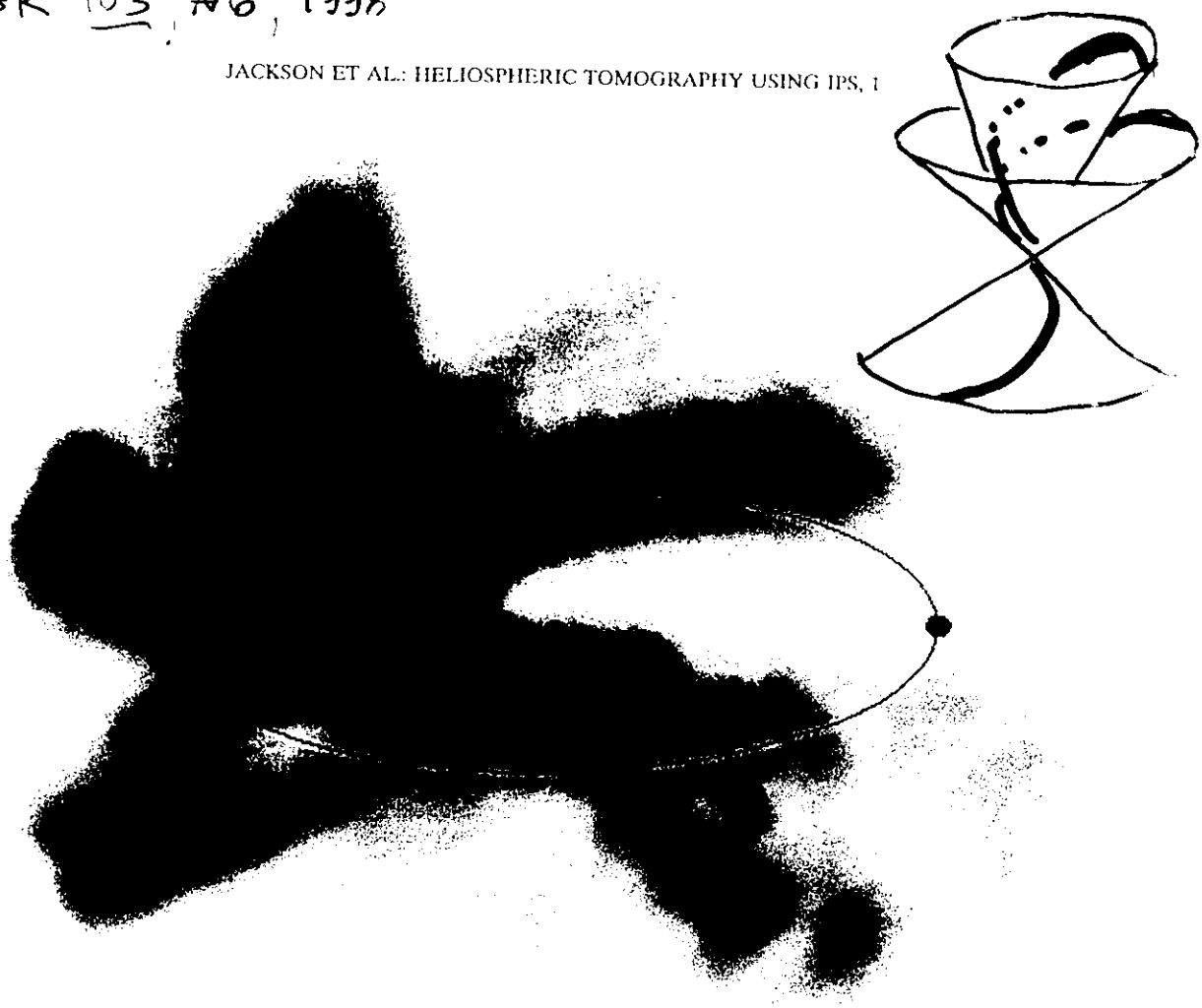

Plate 1. Three-dimensional depiction of density for Carrington rotation 1884 derived by mapping IPS observations to heliocentric distances up to 1.5 AU. Densities are plotted by removing an r^{-2} distance dependence. The Sun is depicted as a dot in the center, and the Earth's orbit, an ellipse with the Earth a dot to the right. The view is from 15° above the heliographic equator at 270° heliographic longitude at the beginning of the Carrington rotation.

$P > 0.5$ from in situ observations at 1 AU for solar wind densities in the range of 5 to 25 e^- cm^{-3}, consistent in general with the Doppler scintillation measurements. However, measurements by *Asai et al.* [1998] determine a result different from that of *Pätzold et al.* [1996]. In the appendix using synthetic data we further explore the manifestations an incorrect assumption of this relationship may have on the tomography.

There are more than an adequate number of IPS sources available to produce the resolution required to map to individual solar features for each solar rotation. The old point P method was more restricted in this sense because although the lines of sight probed regions (over the solar poles, for instance) beyond the point P, there was no way of adequately mapping the features there. Thus point P Carrington maps often only gave good information concentrated close to the heliographic equator and relied on the occasional solar pole crossing of a high ecliptic latitude source to provide information at other than the equator. Often the point P analysis was averaged over periods of 6 months [*Rickett and Coles*, 1991] to show general trends in the data especially at high solar latitudes. This is not as necessary using the tomographic modeling analyses. That there is some evolution over a solar rotation is evidenced by the differences between Carrington maps from one rotation to the next. We are able to separate sources into those which are east of the Sun and those which are west. Although this is a study in itself, we observe some changes from the east-to-west sources that are due to evolution of the structures over times short compared to one solar rotation. We expect this from such studies as *Jackson* [1991] where corotating heliospheric structures are shown to be greatly variable in distance from the Sun. We are also able to restrict IPS sources in the analysis to lie within different elongation ranges from the Sun. So far [*Kojima et al.*, 1997], we have found no significant trends indicating substantial differences for different elongations.

The most significant difference in the tomography result shown in the data projected to the solar surface and to 1 AU is the longitudinal shift of the structures observed. This is nothing more than the continued radial outward solar wind flow from specific regions on the Sun as understood by *Parker* [1958]. These differences can be depicted graphically by projecting the densities to different levels within the three dimensional model as we do for rotation 1884 in Plate 1. To produce this result, Carrington maps are determined from the three-dimensional model at 0.1 AU distances from the solar surface up to 1.5 AU. The structures are fit by the tomographic analysis which enforces strict corotation, and thus they may be highlighted because of it. The density structures would not change much with distance except that the three-dimensional

Nonlinear periodic motions in a gas of noninteracting particles → mixing in the solar wind along B

I. S. Veselovskiĭ

Nuclear Physics Research Institute of the Moscow State University
(Submitted 1 March 1979)
Zh. Eksp. Teor. Fiz. 77, 1352–1359 (October 1979)

An initial-value problem with periodic variation of the velocity in space is solved. The evolution of the density and velocity before and after the "toppling" of the velocity profile is investigated in detail. The formation of discontinuities in the density and in the average velocity after the onset of the multistream flow is traced. The number of mutually penetrating streams increases with time, but the system retains the smallest initial period and the number of density peaks does not increase. For a sinusoidal initial condition there is one density maximum for the period preceding the toppling of the profiled, and after this first toppling there are two density peaks per period, with the exception of individual instants of time when these peaks merge. At long times, the system tends to a homogeneous state throughout, with the exception of some rapidly narrowing regions that preserve the density singularity.

PACS numbers: 05.60. + w, 05.30. − d

1. A cold gas of noninteracting particles is one of the simplest classical systems suitable for simulation of nonlinear motion in continuous media. A qualitative study of this model reveals many processes that are typical also of a more complicated nonlinear system, say a plasma. In such a system, higher harmonics are generated, the slope of the leading fronts increases, "toppling" of the wave profile takes place, and multistream flow with density peaks sets in. The number of mutually penetrating streams increases in the course of the evolution of the process.

A simple and physically illustrative description of some of the main properties of nonlinear motions in such a system can be found in Refs. 1 and 2. However, as will be shown below, a more detailed quantitative treatment helps clarify certain details that refine and modify the picture of the evolution of the nonlinear periodic motions. We consider in detail the case of greatest interest, that of the toppling of the profile. From the qualitative point of view it becomes clear that the shortest period of the motion remains unchanged also after the toppling. After the formation of the multistream flow, the density has two peaks per period. The number of peaks does not increase in the course of the evolution. These two peaks converge into one at definite points of space only at certain individual instants of time. Thus, the purpose of the present paper is to analyze quantitatively the evolution of nonlinear periodic velocity perturbations in a cold gas of noninteracting particles.

We consider the initial-value problem for the plane case. Assume that at the initial instant of time $t=0$ there is specified the distribution function

$$f_0(x, v_x, 0)=n_0(x)\delta(v_x-V).$$

The velocity of the cold gas at the initial instant is

$$V=V_0(1+a\sin kx).$$

The evolution is along the characteristics

$$x=x_0+v_xt, \quad v_x=\text{const}, \quad x_0=\text{const}$$

of the equation

$$\frac{\partial f}{\partial t}+v_x\frac{\partial f}{\partial x}=0.$$

At $t\geq 0$ the solution is the distribution function

$$f(x, v_x, t)=n_0(x-v_xt)\delta\{v_x-V_0[1+a\sin(kx-v_xt)]\}. \quad (1)$$

The particle concentration is

$$n=\int f\,dv_x=\sum_i n_i,$$

where

$$n_i=n_0(x-v_it)\,|1+V_0akt\cos(kx-u_it)|^{-1}. \quad (2)$$

The flux is

$$j=\sum_i j_i=\sum_i u_in_i,$$

and the average velocity $u=j/n$. Here $u_i(x,t)$ are the roots of the equation

$$F(u)=u-V_0[1+a\sin(kx-ut)]=0. \quad (3)$$

At $0\leq t\leq (kaV_0)^{-1}$ Eq. (3) has a single root. The function $u(x,t)$ is in this case single-valued. Putting $(u-V_0)/aV_0=y$, $k(x-V_0t)=\varphi$, and $kaV_0t=p$, we get from Eq. (3)

$$y=\sin(\varphi-py), \quad (4)$$

whence

$$\varphi=\operatorname{Arcsin} y+py=r\pi+(-1)^r\arcsin y+py, \quad r=0, \pm1, \pm2\ldots. \quad (5)$$

Each value of y corresponds to an infinite denumerable set of values of φ at all p. The inverse function $y(\varphi)$ has a finite number of branches at any finite value of p. At $0<p<1$ the function $y(\varphi)$ is single-valued. Its derivative is

$$d\varphi/dy=(-1)^r(1-y^2)^{-1/2}+p.$$

Obviously $|y|\leq 1$.

The extremal values $y=\pm1$ are reached at

$$\varphi=r\pi\pm(-1)^r\pi/2\pm p.$$

The derivative is then $d\varphi/dy=\infty$. The toppling of the profile takes place at points where $d\varphi/dy=0$. This is possible only at odd values of r, when $y=\pm(p^2-1)^{1/2}/p$,

 0038-5646/79/100681-04$02.40

i. e., at the points

$$\varphi = r\pi \pm (-1)^r \arcsin\frac{(p^2-1)^{1/2}}{p} \pm (p^2-1)^{1/2},$$

where $r = 2m+1$, m is any integer, and $p > 0$. It is seen that at $0 < p < 1$ no toppling is possible. The first toppling occurs at $p = 1+0$ at the points $\varphi = (2m+1)\pi$.

3. We introduce the variables $\tau = p-1$, $\psi = \varphi - (2m+1)\pi$ and consider the function $y(\varphi, p)$ near the first toppling, $\tau \ll 1$, $y \ll 1$. Taking into account the periodicity

$$y(\varphi) = y(\varphi + 2\pi),$$

we put $\psi \ll 1$. It follows then from (5) that

$$\psi \approx \tau y - {}^1/_6 y^3 + \ldots .$$

This cubic equation yields $y(\psi, \tau)$. The function $y(\psi)$ is odd and its plots for different values of τ are shown qualitatively in Fig. 1.

a) At $\tau < 0$ the function $y(\psi)$ is single-valued and given by

$$y_1 = 2^{1/2}|\tau|^{1/2} \operatorname{sgn}\psi \operatorname{sh} \ln[\mu + (\mu^2+1)^{1/2}]^{1/3},$$

$$\mu = \frac{3\sqrt{2}}{4}|\psi||\tau|^{-3/2}. \qquad (6)$$

b) At $\tau = 0$ we have

$$y = (-6\psi)^{1/3}. \qquad (7)$$

c) At $\tau > 0$ the function $y(\psi)$ is single valued in the region $\mu < 1$, where it is given by

$$y_1 = 2^{1/2}|\tau|^{1/2} \operatorname{sgn}\psi \operatorname{ch} \ln[\mu + (\mu^2-1)^{1/2}]^{1/3}. \qquad (8)$$

Expression (8) tends to $\tau \to +0$ to (7) in the region $\mu > 1$, and as $\mu \to 1+0$ we have

$$y_1 \to 2^{1/2}|\tau|^{1/2} \operatorname{sgn}\psi.$$

In the region $\mu \leq 1$ at $\tau > 0$ the function $y(\psi)$ is triple-valued:

$$\begin{aligned} y_1 &= -2^{1/2}|\tau|^{1/2} \operatorname{sgn}\psi \cos({}^1/_3 \arccos\mu), \\ y_2 &= 2^{1/2}|\tau|^{1/2} \operatorname{sgn}\psi \cos {}^1/_3(\pi - \arccos\mu), \\ y_3 &= 2^{1/2}|\tau|^{1/2} \operatorname{sgn}\psi \cos {}^1/_3(\pi + \arccos\mu). \end{aligned} \qquad (9)$$

In this region we have as $\mu \to 0$

$$y_1 = -(6\tau)^{1/3} \operatorname{sgn}\psi, \quad y_2 = (6\tau)^{1/3} \operatorname{sgn}\psi, \quad y_3 = 0.$$

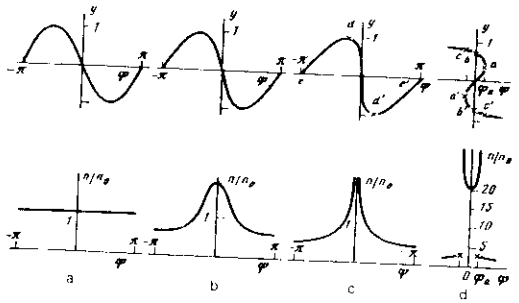

FIG. 1. Evolution of the velocity $y(\psi, \tau)$ and of the density $n(\psi, \tau)$ in the first toppling of the profile: a) $\tau = 0$, b) $\tau = -0.5$, c) $\tau = 0$, d) $\tau = 0.1$.

At $\mu = 1-0$ it follows from (9) that

$$y_1 = -2^{1/2}\tau^{1/2} \operatorname{sgn}\psi,$$

the two other roots merge

$$y_2 = y_3 = (2\tau)^{1/2} \operatorname{sgn}\psi.$$

The branch y_1 at the point $\mu = 1$ (point c in Fig. 1) is continuous and is determined by (9) at $\mu < 1$ and by (8) at μ.

1. The branches y_2 and y_3 exist only at $\mu \leq 1$. The sequence of the branches is shown in Fig. 1: $edcbb'c'd'e'$–the first branch (y_1), $a'b'ab$–second branch (y_2), $a'a$–third branch (y_3). The positions of the points $a-c$ are determined by the approximate formulas (8) and (9). We have

$$\psi_a = {}^1/_3(2\tau)^{1/2}, \quad y_a = (2\tau)^{1/2}, \quad \psi_b = 0, \quad y_b = (6\tau)^{1/3},$$
$$\psi_c = -{}^1/_3(2\tau)^{1/2}, \quad y_c = 2(2\tau)^{1/2}.$$

The coordinates of the points d and e are calculated from the exact formulas (4) and (5):

$$\psi_d = -\pi/2 + 1 + \tau, \quad y_d = 1; \quad \psi_e = -\pi, \quad y_e = 0.$$

The points $a'-e'$ are mirror-symmetrical relative to $a-e$. The density is calculated from (2). Let $n_0 = 1$ in this formula. Then the concentration on each branch is

$$n_i = |1 + p\cos(\varphi - py_i)|^{-1} = |1 + p(-1)^r(1-y_i^2)^{1/2}|^{-1}. \qquad (10)$$

The concentration on the branch ed decreases monotonically with time because of the dilatation of the volume. At the point e we have $n \sim |1+p|^{-1}$ and at the point d we have $n = 1$. At the points $a-c$ ($\psi \ll 1$, $y \ll 1$, $\tau \ll 1$) we can use the expansion

$$n_i \approx |-\tau + {}^1/_2 y_i^2 + {}^1/_2 y_i^4|^{-1}.$$

At the point 0 we have $y_2 = 0$ and on this branch $n_2 \approx |\tau|^{-1}$. At the points c and b we have $y = 2^{3/2}|\tau|^{1/2}$ and $y = (6\tau)^{1/2}$, and correspondingly $n \approx |3\tau|^{-1}$, $n \approx |2\tau|^{-1}$. At the toppling point a we have $\tau \approx \frac{1}{2}y^2$ and the succeeding terms of the expansion must be retained when the concentration is calculated.

We turn therefore to the initial exact expression (5) and consider the vicinity of the toppling points in greater detail. At these points, as already noted,

$$y_* = \pm\frac{(p^2-1)^{1/2}}{p}, \quad \varphi_* = r\pi \pm (-1)^r \arcsin\frac{(p^2-1)^{1/2}}{p} \pm (p^2-1)^{1/2}, \qquad (11)$$

$r = 2m+1$ is odd and $p > 1$. The upper sign corresponds to the point a, and the lower to the point a'. At the toppling points $1 - y_*^2 = 1/p^2$ we have

$$\begin{aligned} \frac{d\varphi}{dy}\Big|_{y_*} &= p + (-1)^r(1-y_*^2)^{-1/2} = 0, \\ \frac{d^2\varphi}{dy^2}\Big|_{y_*} &= (-1)^r y_*(1-y_*^2)^{-3/2} = \pm(-1)^r p^2(p^2-1)^{1/2}, \\ \frac{d^3\varphi}{dy^3}\Big|_{y_*} &= (-1)^r(1+2y_*^2)(1-y_*^2)^{-5/2} = (-1)^r p^3(3p^2-2), \\ \frac{d^4\varphi}{dy^4}\Big|_{y_*} &= (-1)^r 3y_*(3-2y_*^2)(1-y_*^2)^{-7/2} = 3(-1)^r p^4(p^2+2)(p^2-1)^{1/2}. \end{aligned} \qquad (12)$$

We use the obtained values of the derivatives in the expansions

$$\varphi(y)=\varphi_*+\frac{1}{2}\frac{d^2\varphi}{dy^2}\Big|_{y_*}(y-y_*)^2+\frac{1}{6}\frac{d^3\varphi}{dy^3}\Big|_{y_*}(y-y_*)^3+\dots,$$

$$\varepsilon^{-1}=|1-p(1-y^2)^{1/2}|=n_*^{-1}+\frac{dn^{-1}}{dy}\Big|_{y_*}(y-y_*)+\frac{1}{2}\frac{d^2n^{-1}}{dy^2}\Big|_{y_*}(y-y_*)^2+\dots.$$

Putting $y-y_*=\varepsilon$, $\varphi-\varphi_*=\chi$, we obtain near the point a

$$\chi=-\tfrac{1}{3}p^3(p^2-1)^{1/2}\varepsilon^3-\tfrac{1}{4}p^3(3p^2-2)\varepsilon^4+\dots, \tag{13}$$

$$n^{-1}=p^3(p^2-1)^{1/2}\varepsilon+\tfrac{1}{2}p^3(3p^2-2)\varepsilon^2+\dots. \tag{14}$$

The discarded terms are always small compared with the retained ones at $\varepsilon\ll 1$. In the derivation of (14) it was recognized that

$$n_*^{-1}=|1-p(1-y_*^2)^{1/2}|=0.$$

We note that χ is negative here.

In the case $\tau=p-1\ll 1$ we must distinguish between two regions: $|\chi|\ll\tau^{3/2}$ and $|\chi|\gg\tau^{3/2}$. In fact, if $\varepsilon\ll(2\tau)^{1/2}$, then the principal terms in (12) and (13) are the first ones

$$\varepsilon_{1,2}=\pm(-2\chi)^{1/2}(2\tau^{-1/2}),\quad n_{1,2}\approx(|\varepsilon|(2\tau)^{1/2})^{-1}=(-2\chi)^{-1/2}(2\tau)^{-1/4}.$$

These expressions are valid if $|\chi|\ll 2^{1/2}\tau^{3/2}$.

On the other hand if $|\varepsilon|\gg(2\tau)^{1/2}$, then the principal terms will be the second ones. Then $\varepsilon_1\approx(-6\chi)^{1/3}$, $n_1\approx 2\varepsilon_1^{-2}=2(-6\chi)^{-2/3}$. These expressions are valid at $|\chi|\gg 2^{1/2}\tau^{3/2}$, and in particular at $\tau=0$. We indicate here the subscript that numbers the branch.

Thus, at the instant of the first toppling at $\tau=0$, $\varphi=(2m+1)\pi$ the density has only one singularity of the type $n\sim\chi^{-2/3}$ over the entire period at the toppling point ($\chi=0$). In the subsequent instants of time $0<\tau<1$ there are two toppling points (a and a') in the period, as well as a density singularity of the type

$$n\sim|\chi|^{-1/2}\tau^{-1/2}$$

in the immediate vicinity on the left of the point a (on the right of a') at $|\chi|\ll 2^{1/2}\tau^{3/2}$. At the points e and e' the density equals $1/(2+\tau)$, while at the points d and d' the density is not distorted, $n=1$. At the toppling point $\psi_*=\psi_a$ on Fig. 1 the density has a discontinuity: On the right there is one branch $n\approx\frac{1}{3}\tau$. To the left of this point there are three and the density becomes infinite like

$$n\approx 1/3\tau+2(2\chi)^{-1/2}(2\tau)^{-1/4}$$

in the region

$$|\chi|\ll 2^{1/2}\tau^{3/2}.$$

The average velocity, determined by the ratio

$$\bar u=\sum_i u_i n_i\Big/\sum_i n_i,$$

becomes discontinuous at the toppling points. It assumes successively the values V_0 at the point e, $(1\pm a)V_0$ at the point ψ_d, $V_0(1+2^{1/2}a\tau^{1/2})$ at the point ψ_c-0, $V_0(1-2^{1/2}a\tau^{1/2})$ at the point ψ_c+0, V_0 at the point 0, $V_0(1+2^{1/2}a\tau^{1/2})$ at the point ψ_a-0, $V_0(1-2^{1/2}a\tau^{1/2})$ at the point ψ_a+0, etc. (see Fig. 2). The jump of the average velocity at the toppling points is $\pm 3\times 2^{1/2}aV_0\tau$, $\tau\ll 1$. It increases with time and tends to the value $\pm aV_0$ as $t\to\infty$.

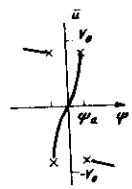

FIG. 2. Average velocity $u(\psi)$ after toppling ($a=0.1$, $\tau=0.1$, $V_0=1$, $\psi_a=3\cdot 10^{-2}$).

For each branch we can write everywhere, with the exception of the toppling points, the expansions

$$y(\varphi)=y(\varphi_a)+\frac{dy}{d\varphi}\Big|_{\varphi_a}(\varphi-\varphi_a)+\frac{1}{2}\frac{d^2y}{d\varphi^2}(\varphi-\varphi_a)^2+\dots,$$

$$n(\varphi)=n(\varphi_a)+\frac{dn}{d\varphi}\Big|_{\varphi_a}(\varphi-\varphi_a)+\frac{1}{2}\frac{d^2n}{d\varphi^2}(\varphi-\varphi_a)^2+\dots. \tag{15}$$

The functions $y(\varphi)$ and $n(\varphi)$ are implicitly specified here by Eqs. (4) and (10), and the derivatives are

$$\frac{dy}{d\varphi}=G^{-1}\cos(\varphi-py)=(-1)^r(1-y^2)^{1/2}G^{-1},$$

$$\frac{d^2y}{d\varphi^2}=G^3y,\quad \frac{dn}{d\varphi}=pyG^{-3}\operatorname{sgn}G, \tag{16}$$

$$\frac{d^2n}{d\varphi^2}=[p\cos(\varphi-py)G^{-4}+3p^2y^2G^{-3}]\operatorname{sgn}G.$$

To simplify the formulas, we have introduced the notation

$$G=1+p\cos(\varphi-py)=1+(-1)^r p(1-y^2)^{1/2},\quad n=G^{-1}$$

and have left out the subscript that numbers the branches.

We introduce the symbol $\chi=\varphi-\varphi_a$ and consider the characteristic points anew. At the point e we have $\varphi_e=r\pi$, with r odd,

$$y_e=\sin(\varphi_e-py_e)=0,\quad \cos(\varphi_e-py_e)=1.$$

We obtain

$$y_e\approx(1+p)^{-1}\chi+O(\chi^2),\quad n\approx(1+p)^{-1}+\tfrac{1}{2}p(1+p)^{-4}\chi^2+\dots.$$

At the point d we have $y_d=1$, $\varphi_d=r\pi+(-1)^r\pi/2+p$. This point moves at constant (highest) velocity. About this point we have the expansion

$$y=1-\tfrac{1}{2}\chi^2+\dots,\quad n=1+p\chi+\tfrac{1}{2}p^2\chi^2+\dots.$$

At the points c and b we obtain a transcendental equation for $y(p)$. These points were considered at $\tau\ll 1$. At the toppling point a the expansion (15) is not suitable ($G=0$). At the point 0 the phase is $\varphi=r\pi$, r is odd, $y=0$, and $G=1-p$. The expansions at these points are given by

$$y=(p-1)\chi+O(\chi^2),$$

$$n=|p-1|^{-1}+\tfrac{1}{2}p(p-1)^{-2}\operatorname{sgn}(p-1)\chi^2+O(\chi^3).$$

5. The behavior near the toppling points is described by Eqs. (13) and (14), from which we get as $t\to\infty$ the asymptotic expressions

$$\varepsilon=(2\chi)^{1/2}p^{-3/2},\quad n=(2\chi)^{-1/2}p^{-1/2},$$

if $p^2\varepsilon\ll 1$, i.e., in the region $(\chi p)^{1/2}\ll 1$. On the other hand, if $p^2\varepsilon\gg 1$, then

$$\varepsilon=(2\chi)^{1/2}p^{-1/2},\quad n=\tfrac{2}{3}(2\chi)^{-1/2}p^{-1/2},$$

in the region $(2\chi p)^{1/3}\gg 1$. Thus, the density singularity

continues to exist at all time when $p>1$, but narrows down rapidly.

As $t\to\infty$, $\varphi\approx -kV_0 t\to\infty$ we get $y_r\approx(\varphi-r\pi)/p$. Since $-1<y<1$, we get for integer r the restriction $r_{\min}<r<r_{\max}$, where $r_{\min}=p(1-a)/\pi a$, $r_{\max}=p(1+a)/\pi a$. The number of mutually penetrating streams $N=r_{\max}-r_{\min}=2p/\pi$ increases linearly with time.

The concentration of each stream is

$$n_r=|1+p(-1)^r(1-y_r^2)^{1/2}|^{-1}\approx p^{-1}(1-y_r^2)^{-1/2}.$$

The density is calculated by summing over r, which can be replaced by integration over the equidistant spectrum y_r, with $\Delta y_r=y_{r+1}-y_r=\pi\Delta r/p$:

$$n=\sum_{r_{\min}}^{r_{\max}} n_r=\int_{r_{\min}}^{r_{\max}} n_r\,dr=\int_{-1}^{1} n(y)\frac{p}{\pi}dy=\frac{1}{\pi}\int_{-1}^{1}(1-y^2)^{-1/2}dy=1. \quad (17)$$

At $t\to\infty$ it is natural to regard the quantity

$$f(y)=\begin{cases}\pi^{-1}(1-y^2)^{-1/2}, & |y|<1\\ 0, & |y|>1\end{cases} \quad (18)$$

as the velocity distribution function with normalization (17). The average velocity is

$$\langle y\rangle=\int yf(y)dy=0,$$

The mean squared velocity of the "thermal" motion is

$$\langle y^2\rangle=\int y^2 f(y)dy=\frac{1}{2}.$$

Thus, with the exception of narrow regions containing density singularities, the system evolves into a homogenous state with a distribution function (18), characterized by a density $n=1$, an average stream velocity $u=V_0$, and an effective temperature

$$T_{\text{eff}}=\frac{m}{2}\langle(u-V_x)^2\rangle=\frac{m}{4}(aV_0)^2.$$

Allowance for the thermal motion in the initial distribution (1) leads to a spreading of the inhomogeneities and to a finite amplitude of the density peaks. The equilibrium velocity distribution is established when account is taken of the collisions. Motions of the considered type are possible in a plasma consisting of cold ions and thermal electrons (see, e. g., Refs. 3 and 4), in which case the potential is

$$e\varphi=T_e\ln(n/n_0).$$

The author thanks V. I. Karpman and L. P. Pitaevskiĭ for helpful discussions.

[1]B. B. Kadomtsev, Kollektivnye yavleniya v plazme (Collective Phenomena in Plasma), Nauka, 1976, Ch. 3.
[2]B. B. Kadomtsev and V. I. Karpman, Usp. Fiz. Nauk 103, 193 (1971) [Sov. Phys. Usp. 14, 40 (1971)].
[3]I. A. Akhiezer and A. E. Borovik, Zh. Eksp. Teor. Fiz. 51, 1227 (1966) [Sov. Phys. JETP 24, 823 (1966)].
[4]A. V. Gurevich and L. P. Pitaevskiĭ, Zh. Eksp. Teor. Fiz. 56, 1778 (1969) [Sov. Phys. JETP 29, 954 (1969)].

Translated by J. G. Adashko

Self-action of electromagnetic waves in a plasma subject to modulational instability

A. G. Ltvak, V. A. Mironov, and A. M. Feĭgin

Institute of Applied Physics, Academy of Sciences of the USSR
(Submitted 5 April 1979)
Zh. Eksp. Teor. Fiz. 77, 1360–1366 (October 1979)

We study the nonlinear penetration of an electromagnetic wave into a plasma upon development of modulational instability. We use an averaging method which employs the substantial scale difference between the plasma and the electromagnetic waves to find the change in the refractive index of the incident wave when the plasma is layered on a fine scale. We consider in detail the stationary self-action of an s-wave in an initially uniform layer of an overdense plasma with sharp boundaries. We find the field distribution and the dependence of the transmission coefficient on the amplitude of the field of the incident wave.

PACS numbers: 52.35.Hr, 52.35.Py, 52.40.Db

INTRODUCTION

It is well known that the processes of the modulational instability of Langmuir waves, which lead to the formation of Langmuir solitons and of the corresponding inhomogeneities in the plasma density (cavitons), play an essential role when strong electromagnetic waves interact with a dense collisionless plasma. One usually studies the modulational instability in order to determine the magnitude of the effective collision frequency ν_{eff} which characterizes the additional electromagnetic-energy loss connected with the excitation of fine-scale electric fields. In that case one does not take into account the fact that appearance of cavitons (plasma stratification) also leads to a change in the real part of the refractive index of the electromagnetic wave and, thereby, to a change in the distribution of the large-scale electric fields in the plasma. It is clear that taking such "reactive" non-linear effects into account is important for the determination of the characteris-

0038-5646/79/100684-04$02.40

Large-scale solar wind stream structure at high heliolatitudes

I. S. Veselovsky
Institute of Nuclear Physics
Moscow State University

Introduction

- Tilted rotator model /Zhao & Hundhausen, 1981
- Gaskinetic approximation /Veselovsky, 1980, 1981/

$M, M_A \gg 1$

Simple model

$$\frac{\partial f}{\partial t} + \vec{v}\frac{\partial f}{\partial \vec{r}} = 0$$

$$V = V_0 (1 + a \cos^2 \theta_m)$$

during the declining solar cycle phase

$$r = r_0 + \int_{t_0}^{t} V_0(\theta, \varphi, t')\, dt'$$

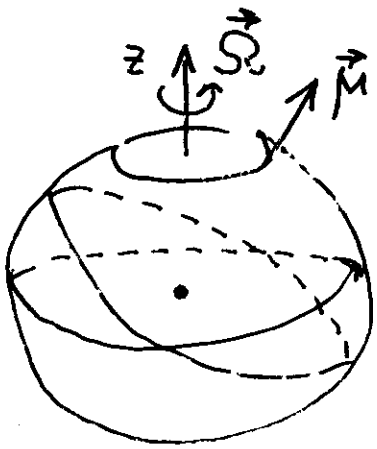

Heliographic equator

Heliomagnetic equator

- $\vec{r}(r, \theta, \varphi)$ observational point, [illegible]

Stream Structure.

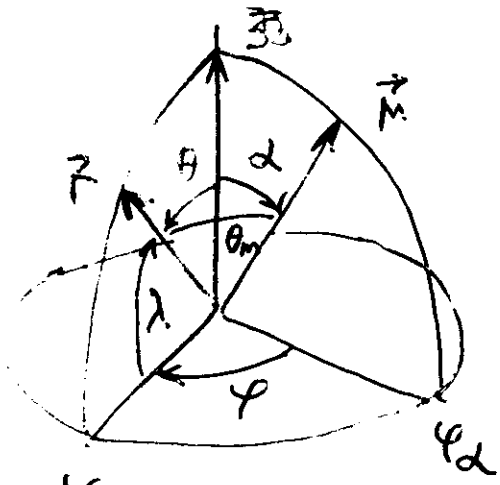

Extremal points:

$$\frac{\partial V}{\partial \theta} = 0$$

$$V_{max} = V(1 + a\cos^2(\theta - \alpha)) \quad \begin{matrix} 0 < \theta < \pi/2 - \alpha, & \varphi = 0; \\ \pi/2 - \alpha < \theta < \pi, & \varphi = \pi. \end{matrix}$$

$$V_{min} = V \begin{cases} 1 & \theta_m = \pi/2, \\ 1 + a\cos^2(\theta + \alpha) & \end{cases} \quad \begin{matrix} \pi/2 - \alpha < \theta < \pi, & \varphi = 0; \\ 0 < \theta < \pi/2 - \alpha, & \varphi = \pi. \end{matrix}$$

$$\Delta V = aV \begin{cases} \sin^2(\lambda + \alpha), & 0 < |\lambda| < \alpha, \\ \sin 2\lambda \sin 2\alpha, & \alpha < |\lambda| < \pi/2. \end{cases}$$

Case 1) $\alpha \leq \pi/4$

max $\Delta V = aV \sin 2\alpha$ when $\lambda = 45^\circ$

Case 2) $\alpha \geq \pi/4$

max $\Delta V = aV$ when $\lambda = \pi/2 - \alpha$

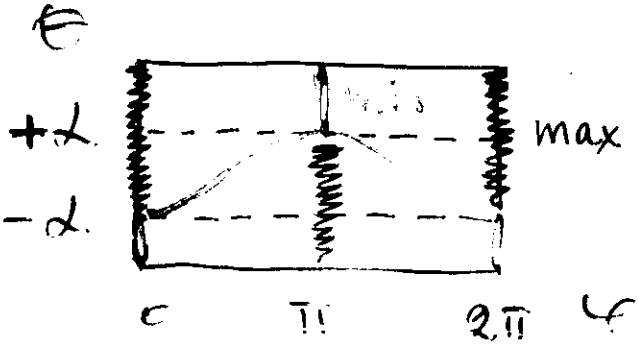

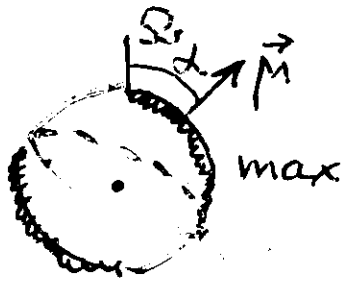

The Sun as a Star

Radius $R_\odot \sim 0{,}7\,GM$ (695 970 km)

Mass $M_\odot \sim 2 \cdot 10^{33}$ g $(1{,}989 \cdot 10^{33})$

Infrared & visible luminosity $S_\odot \sim 3.85 \cdot 10^{23}$ kW

Age $\sim 4.7 \cdot 10^9$ years

$T_{CENTER} \sim 15$ MK

$T_{surface} \sim 6000$ K

Rotation $\frac{\Omega}{2\pi} \sim 380 - 480$ nHz

(Period ~25 days at the equator)
~35 days at 70°

1 AU $\sim 1{,}5 \cdot 10^{13}$ cm

Solar flare (R. Hodgson 1 sept. 1860)
eye-sketch
now: stellar activity, flares

Spectroheliograph (G.E. Hale, 1908)
B in spots ≤ 4.5 kG (1913)
now: stellar magnetic fields

Radiative equilibrium (K. Schwarzschild 1906)

Hydrogen + 10% He + few percent of all others

Nuclear Reactions

Proton chain

$$p + p \rightarrow {}^{2}H + e^{-} + \nu_e$$

$${}^{2}H + p \rightarrow {}^{3}He + \gamma \qquad 12,86\ MeV$$

$${}^{3}He + {}^{3}He \rightarrow {}^{4}He + p + p$$

or

$${}^{3}He + {}^{4}He \rightarrow {}^{7}Be + \gamma \qquad 17,35\ MeV$$

$${}^{7}Be + e^{-} \rightarrow {}^{7}Li + \nu_e$$

$${}^{7}Li + p \rightarrow {}^{8}Be + \gamma + {}^{4}He + {}^{4}He$$

Carbon chain

$${}^{12}C + p \rightarrow {}^{13}N + \gamma$$

$${}^{13}N \rightarrow {}^{13}C + e^{-} + \nu_e$$

$${}^{13}C + p \rightarrow {}^{14}N + \gamma$$

$${}^{14}N + p \rightarrow {}^{15}O + \gamma$$

$${}^{15}O \rightarrow {}^{15}N + e^{-} + \nu_e$$

$${}^{15}N + p \rightarrow {}^{12}C + {}^{4}He$$

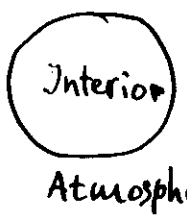

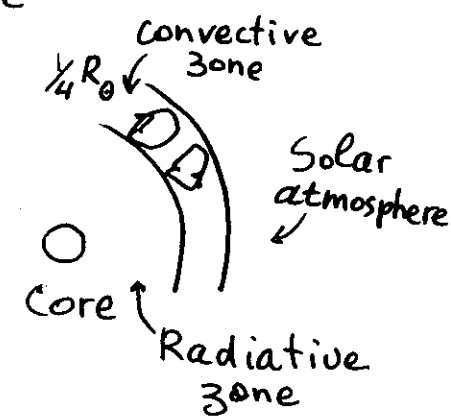

Woltjer (1965):

— Are stellar magnetic fields a surface phenomenon? No

Magnetic fields and electric currents are present above the surface, everywhere and every time in the solar atmosphere. What are $\vec{B}(\vec{r},t)$ and $\vec{j}(\vec{r},t)$ inside?

— Why are stellar magnetic fields variable?

rotation, internal convection, finite σ

— How are prominences kept in equilibrium?

They are NOT in equilibrium.
They are OPEN systems (NOT CLOSED!) with mass flows.
Quasi-steady-states are possible (quiescent prominences).
They gain and loss the mass even in the quasi-steady state.
The replenishment time t (hours, days) could be small or large in comparison with the life-time T of the corresponding magnetic configuration, which is responsible for the visual shape

Prominences are multi-scale in space and time

About the Heliosphere

1) "Physics of the Inner Heliosphere"
Eds. R. Schwenn, E. Marsch, Springer-Verlag,
1. Large-Scale Phenomena 1990
2. Particles, Waves and Turbulence 1991

2) "The heliosphere in the Local Interstellar medium", Eds. R. von Steiger, R. Lallement and M.A. Lee.
Space Sci. Rev., 78, #1-2, 1996

3) "Cosmic winds and the heliosphere"
Eds. Jokipii J.R., Sonett C.P., Giampapa M.S.
Univ. of Arizona Press, Tucson, 1997

4) "Solar wind EighA"
AIP Press, 1996

5) http://nssdc.gsfc.nasa.gov/omniweb/spdf
//spds.nasa /coho
//umbra.gsfc.nasa gov/sdac.html
//alpha.npi.msu.su/~alla

6) "Solar Wind Nine". AIP Press. 1999

Helios 1, 2.
Pioneer 10, 11
Voyager 1, 2
0.3 ~ 70 AU

Wind
ACE

Ulysses
SoHo